Bachelor Thesis

Bachelor's Degree in

Industrial Technology Engineering

Study and Program for an F2A Category Control Line Speed Model

REPORT

Author: Carlos Ebrahim Vendrell

Director: Lluís Roger Casals

Call: June 2018

Escola Tècnica Superior
d'Enginyeria Industrial de Barcelona

I. Abstract

This thesis sets out to study as many variables of the flight of an F2A Speed category control line model as possible. An Excel program has been created together with this report to allow enthusiasts to test the parameters of their models and quickly determine what their performance will be, in terms of drag and lift forces involved, stretching of the control lines and required engine power.

As an example, a concrete study has been developed around a world record breaking model, *Barcelona 96,* owned by a local former world champion, Lluís Parramón. Throughout the thesis, the performance of this model will be studied in depth, identifying its optimal angle of attack once in a steady state sustained flight., the lift force this angle produces and the effect it has on the model`s drag.

Apart from the drag force generated by the model, it will be proven that the drag produced by the long, thin, control lines are a much greater concern, as they end up accounting for most of the total drag. Many integration techniques will be used once equations relating differential drag forces for each of the model's sections has been found. Furthermore, the shape the lines acquire due to the forces they are submitted to will be plotted, in all three directions they can deform.

Lastly, a study of the pitching moment of the model will be carried out to be able to tell where the centre of gravity should be placed, and how to solve the problem of pitching if little liberty is had over the choice of the centre of gravity's placement.

The results of the study hope to provide clear optimal values for all three flight angles of the model, together with a compilation of forces it is submitted to. Furthermore, the speed which would be recorded in official timed event has also been computed as it varies depending on the stretch of the control lines.

II. Table of Contents

III. Glossary

Chapter 1: Introduction

Global coordinate system
X: Distance from the flight centre (Radius) [m or mm]

Chapter 2: Boundary Conditions

ρ = Density [Kg/m^3]
P = Pressure [KPa]
M = Molar mass [g] (for air: 28,96g)
R = Gas Constant [8,314 J/K·mol]
T = Temperature [K]
T^R = Temperature [R]
T_o = Reference Temperature (524,07 ºR
μ = Dynamic Viscosity [Pa · s]
μ_o = Reference Viscosity (1,827E-5 Pa · s) at reference temperature T_o
C = Sutherland's constant (120)

Chapter 3: Aerodynamic Lift

Fc = centripetal force [N]
L = Lift [N]
W = Model weight [N]
p = Total line weight [N]
q = Distributed weight of the line [N/m]
θ = Flight Angle [rad]
A_T =Total projected area of wing and stabilizer [m^2]

Chapter 4: Aerodynamic Drag

R = Flight Radius [m]
σ = Stress [Pa]
ε = Strain
y(x) = Deviation from straight flight radius [m]
a = Acceleration of each line section [m/s^2]
L = Length of the arched lines [mm]

Chapter 5: Gyroscopic Momentum

AC = Aerodynamic Centre
$X_{aerofoil}$ = Distance from the wing's leading edge [mm]

IV. Foreword

a. Motivation

As someone who has always been intrigued by various transport systems such as the automotive industry, railway networks and aviation, the latter seemed like the perfect way to combine different fields of mechanics which I've found engaging during this Bachelor's Degree in Industrial Technology Engineering.

However, aviation modelling is a parallel field to aviation that has not been studied as thoroughly, probably from the lack of economic benefit one can obtain. Nevertheless, aeromodelling, can often contain just as many fields of engineering worth studying as commercial aviation, and sometimes include variations like control line with characteristics that are unequalled in any other commercial transport.

For this reason, control line, a way of flying scaled aircraft models in circles using a pair of wires attached to a handle, seemed like a topic worth focusing around, due to its similarities to aviation, but also due the challenge of circular flight. As I continued to research about control line in general, I found out that, with a couple of exceptions, most websites and studies seemed outdated, with flashy colour-contrasted web pages and expired links to other non-existent sites.

I believe that this is mainly due to the age group engaged in control line. As with many other modelling hobbies, often it is the older generations that have time to take part in such competitions for fun, since it is practically impossible to live off such competitions professionally. For this reason, many calculations and studies have been done traditionally, either by hand or in early versions of computers, with outdated programming languages. All of this added extra motivation to contribute to modernizing aeromodelling in general, perhaps engaging younger generations to participate if they could find more recent studies online.

In order to contribute, this thesis has the goal of studying as many variables from an F2A category control line plane. The choice of this category (Speed) inside of control line was due to the possibility to have an enthusiast of F2A as a mentor for this thesis work and furthermore also having the chance to meet with a local F2A pilot, Lluís Parramón, not only an enthusiast, but a multiple time world champion in this category.

With all the studies carried out, an Excel Worksheet will be created, where different parameters can be modified in order to calculate the performance of various models, without the need for developing new worksheets every time. This hopes to contribute in engaging more enthusiasts to try out different combinations and settings of their models, and thus engaging the general public in these competitions worldwide.

For this concrete study, the parameters of Lluís Parramón's world championship winning F2A model will be used, *Barcelona 96*, and it will show how a careful study of its performance can be just as important or even more so than using innovative technologies in order to achieve the maximum speed, the goal of this category.

b. Goal and Scope

Control Line modelling, when competing at the level of national and international championships can result very costly. Usually, parts are specifically designed for control line, so keeping spare parts might result expensive. Due to this, it is optimal to study well in advance the characteristics each customized model will have, as one can only hope to break records and win competitions with custom built models. There are little to none pre-built models for sale, usually second hand, and one of the purposes of control line is also to understand the behaviour of your model and try to combine the best parts for it to work optimally.

The costly thing to do, would be to buy a range of parts including engines, wings, propellers, etc. and try out different combinations in order to see which combination works best. Evidently, this is not just expensive, but also time consuming. This is one of the main goals of this thesis, to give competitors a chance to try out as many configurations and try to predict what the performance of their model would be like in competitions. This is why each section can be modified independently in the Excel worksheet, so the whole study doesn't have to be carried out again if, for example, the shape of the wing changed.

For this reason, the language chosen for this thesis has been English, in order to reach the maximum number of potential of users of the Excel program. It is worth noting that currently, there are many national associations for control line, one of the most relevant being the North American Speed Society, and for that reason many championships are held in the USA, which also has a strong number of enthusiasts.

c. Previous Requirements

This thesis, as stated previously, combines many different subjects taught throughout the Bacherlor's Degree in Industrial Technology Engineering. It is worth mentioning however, that the subjects related to mechanical engineering are of strict relevance. For example, *Basic Mechanics* is important to understand how different forces like wire tension and centripetal force, among others, interact with each other, thus resulting in the acceleration of the model and various moments. Mechanics introduces the concept of the gyroscopic effect and conservation of angular momentum which are theorems which gain importance when flying on a circular path, as is the case in control line. Like in any aviation related study, *Fluid Mechanics* is crucial to understand the lift and drag forces involved and comprehend how the model is kept in flight. Also, the use of thin steel wires for control line makes *Continuum Mechanics* and *Strength of Materials* relevant, in order to study their stretch and behaviour under certain tension. Finally, apart from all the mathematical knowledge needed in all the aforementioned subjects, obtained through various *Calculus* and *Algebra* related courses, *Engineering Drawing* can result useful for calculating inertia moments which otherwise would have to be done by hand and would result much more ponderous. These CAD models could also be simulated using software once the theory behind these, has been comprehended using *Continuum Mechanics* and *Strength of Materials*.

1. Introduction

1.1. F2A Control line

Control Line model flying doesn't have an extensive history, as the first generally recognized flights of a similar system date back to June 1936, by Oba St. Clair. Two-wire control line modelling was not developed until the early forties, when Jim Walker developed and patented this idea. To have an idea of what models could look like back then, Figure 1.1 shows an image of one of Walker's early patented models, which used the third line as an early ignition speed control (D. Macy, 1990).

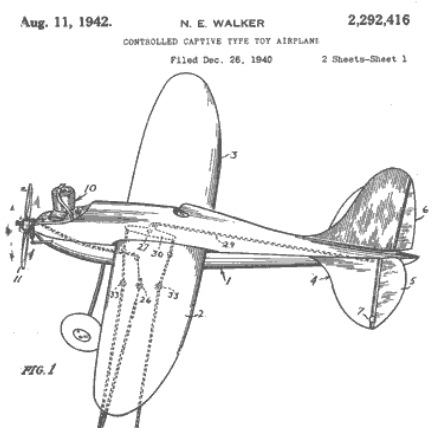
Aug. 11, 1942. N. E. WALKER 2,292,416
CONTROLLED CAPTIVE TYPE TOY AIRPLANE
Filed Dec. 26, 1940 2 Sheets-Sheet 1
FIG. 1

Figure 1.1. One of Jim Walker's first patented models from 1940. American Junior Classics.

During the 50s, in what became the Golden Era of modelling, the diversification of designs contributed to models being focused on achieving different goals, thus leading to competitions. Unlike radio controlled aircraft models, control line models became more competition oriented, and thus the four main categories formed: Speed, Racing, Precision and Combat. For these categories, the international classes are nowadays known as F2A, F2B, F2C and F2D respectively and they have had sporting codes continuously updated; but their main goal still remains the same (G. Olsson, 2013):

F2A Speed: In this class, engine capacity is limited to 2,5cm^3 and the theoretical flight radius is 17,69m (much of the work in this thesis will be in order to give a precise measure of this length). The goal is to complete 9 laps of the circular circuit (1km) in the briefest time possible, thus aiming for the highest speed. Such speeds can reach up to 300km/h so the aerodynamic forces involved need to be studied in great detail in order to maximize the efficiency.

F2B Aerobatics: What is also known as Stunt Class, consists in the performance of complex manoeuvres, usually with bigger and more elaborated models. These models reach up to 85km/h and there is more flexibility in the engine capacity, from 5.6 to 10cm^3 as the goal of this category is more about precision and aesthetics rather than being fast.

F2C Team Racing: Contrary to the previous categories, in this class, the pilot and his mechanic compete as a team in order to complete a course of 100 laps, 10km. Since the fuel tank size is limited to 7cm^3, the need for 2 or 3 pit stops during the race is needed, and that's when the importance of the mechanic comes into play. Speeds of around 200km/h are reached and what makes this category stand out from the rest is that three pilot and mechanic pairs race against each other on the same course at the same time. One might think that this would cause lines to tangle with each other, but since this usually ends in the destruction of the model, pilots are extremely careful to keep a safety distance. Once again, since speed is crucial, engine capacity is limited to 2.5cm^3.

F2D Combat: This category also takes place with multiple pilots on the course. In this case, two pilots (and their two mechanics) compete with a paper tail attached to their models. The goal is to cut the opponent's tail with the model's propeller, and stay in flight. As one might expect, the carnages are common, so each pilot should compete with a handful of spare models, to compensate for crashes. Speeds in this category can reach up to 140km/h, so the crashes can be quite spectacular.

As mentioned previously, the case at hands contemplates the study of an F2A category model. This model, *Barcelona 96*, established the world record for its category in the 1996 world championships, with an official speed of 311,2km/h. However, this record was under an older regulation, so lines of 15,92m were used and 10 laps were timed, despite the total distance of 1k remained the same. In order to increase drag force and reduce the speed of the models, which was deemed too great, longer lines were later enforced. On the current 17,69m lines, it also established a world record in 2002, of 302,5km/h, therefore this speed will be used in its study. To have a sense of how much control line has evolved since then, the current world record holder is Ken Morrissey, who set the bar at 307,4km/h in 2011.

1.2. Dimensions and Regulations

The organization in charge of establishing all control line regulations is the FAI Aeromodelling Comission (CIAM – Comité International d'Aéromodelisme), a division of the World Air Sports Federation. This organization is not only responsible for establishing such regulations, but also for conducting championships and keeping track of world records. The technical regulations involving the dimensions most relevant for this project work are the following (Note that units have not been standardized as they have been kept the same way they are mentioned in the sporting code):

Extract from FAI Sporting Code, Section 4 - Aeromodelling, Volume F2, Control Line Model Aircraft, 2018 Edition:

4.1.1. Definition of a Speed Model Aircraft

Model aircraft in which the power is provided by a piston motor and in which lift is obtained by aerodynamic forces acting on the supporting surfaces, which remain fixed in flight except for control surfaces.

4.1.2 Characteristics of a Speed Model Aircraft

Maximum swept volume of motor or motors .... 2.5 cm^3
Minimum total projected area..... 5.0 dm^2
Maximum total projected area..... 6.0 dm^2
Maximum loading ..... 100 g/dm^2
Maximum wingspan ..... 100 cm

To determine the wingspan of asymmetric model aircraft the thrust line of the model aircraft is used. (…)

4.1.4. Control Lines

a) Only two-line control is allowed; minimum control line diameter is 0.40 mm with a tolerance of minus 0.011 mm.

b) No intentional twisting and/or linking of the two lines together shall be permitted from the point of exit of the model aircraft to the control handle. The lines shall be separated by at least 5 mm at the point of exit from the model aircraft and at least 25 mm at the handle.

c) The lines must be round in cross-section and may not have any liquid or coating material applied. Solvent may be applied for cleaning only.

As can be seen, regulation contemplates an asymmetrical model, and even though it is not compulsory, it has been found to be more effective to use a single wing (usually just under 1m long), instead of flying a symmetrical two-winged model.

This is only true for *F2A* category planes, where the simple trajectory of the model together with the importance of drag reduction in order to increase speed, makes a long inboard wing optimal. For this reason, the wingspan and projected area of the wing is so restricted in the regulations.

Another curious aspect of the regulation is the need for the two control wires to be kept separate, as tangling them together would decrease their overall influence in drag. As it will be demonstrated, the majority of the total drag comes from the wires, despite their thin dimensions.

As the model in this study is an F2A speed model, it follows these asymmetrical characteristics, with a long (960mm) inboard wing. A wide range of dimensions and cross sections can be seen below, in Figure 1.2.

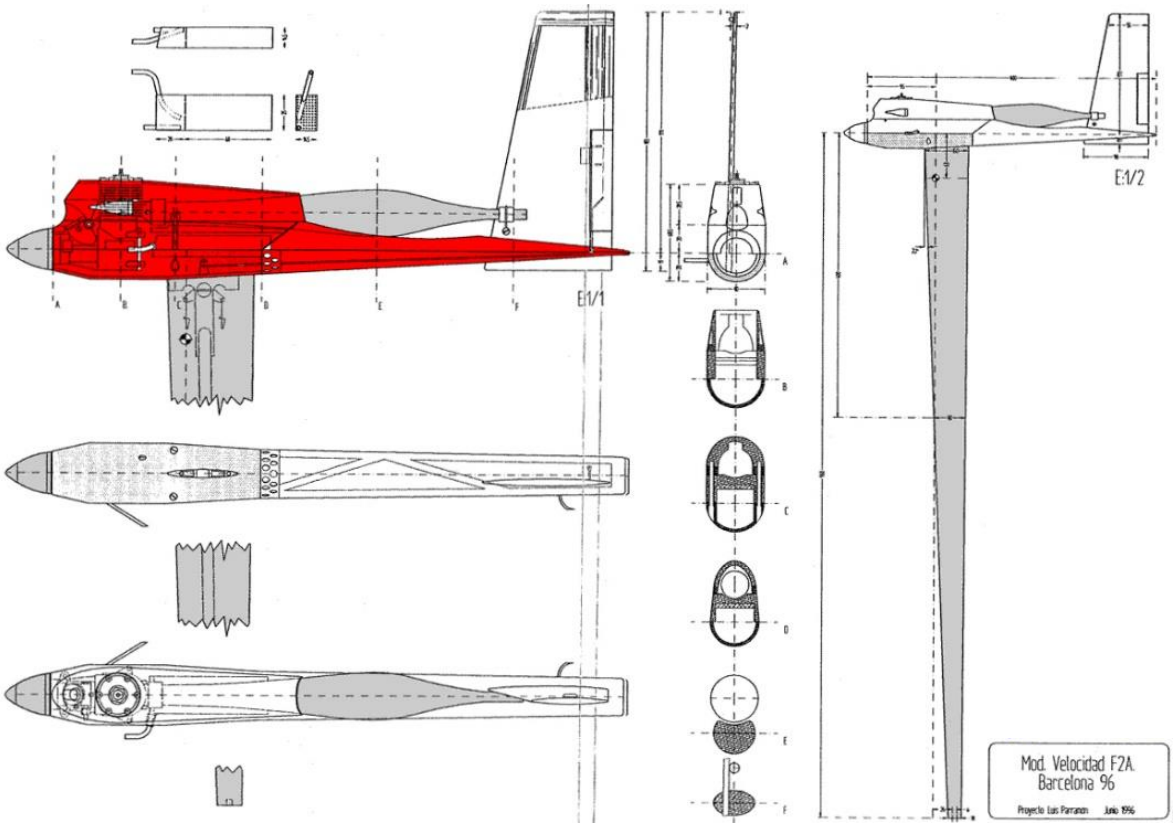

Figure 1.2 Lluís Parramón's winning model, Barcelona 96.

The most relevant dimensions will be introduced into the Excel program specifically created for this project.

1.2.1. Brief User's Manual for the Excel Worksheet Program

Throughout the thesis, screenshots of parts of the program will be shown, in order to be able to easily relate what is being explained and how the calculations would be done using the Excel worksheet.

This worksheet, includes various tabs relating to different parts of the study, these are: Input, Lift, Drag, Power, Yaw, Arching, Inertia and Output. Most of the relevant data will be introduced in the Input tab, however, the other tabs also include cells that need to be modified in case the model being studied changes. Nevertheless, much of the data used in every tab is directly referenced from the Input tab. In this tab, cells have been protected with a valid interval for different reasons, for example:

· Values which could be introduced in the wrong units (m or mm) have been limited to reasonable measures to avoid possible errors.

· Values which are strictly delimited by FAI regulations have had these limitations implemented as the interval in which the values are considered valid.

As a guide, cells which values need to be introduced manually, have a white background with a thick border and cells which values have been calculated by the program, do not (they can vary in colour).

So for the dimensions, there is a section under the tab *Input* of the worksheet to introduce these variables for the model and the wires. For the practical case at hand, these would result in the following Tables 1.3 and 1.4 respectively.

Model: Barcelona 96		
Aerofoil	NACA 0012	
Fuselage Width	50	mm
Wingspan	960	mm
Wing Chord at tip	18	mm
Wing Chord at base	60	mm
Stabilizer Span	170	mm
Stabilizer Chord at base	90	mm
Stabilizer Chord at tip	55	mm
Model Mass	0,42	Kg
Wing Area	3,65E-02	m^2
Stabilizer Area	1,23E-02	m^2
Centre of Gravity	17,627	m

Table 1.3. Model Dimensions Input

Lines		
Number of Lines	2	
Length (until axis)	17,690	m
Length (until CG)	17,627	m
Length (until Wing)	16,730	m
Diameter	4,00E-04	m
Section	1,26E-07	m^2

Table 1.4 Line Dimensions Input

As stated, note that the cells with a white background are for introducing data from the model, while the cells with a grey background correspond to values which are automatically calculated by the program, or unchangeable due to the federation's regulations.

For the lines (Table 1.4), there are different values for the length of these. Sporting regulations establish the length to be calculated from the centre of the flight radius to the axis of thrust, but due to the asymmetry of the model, its centre of gravity is not located along the axis of thrust, it is within the wingspan. In order to study mechanical behaviour and performance, it is important to know the distance of from the centre of flight radius to the centre of gravity (CG), so hence the importance of that cell. Furthermore, the lines are only exposed to drag force when they are not inside of the wing, so for this reason the length of the lines until the wingtip has also been calculated.

As for the engine, it is a Profi Speed, manufactured in Ukraine, which incorporates many characteristics that allow for its tuning. For example, for this model, the engine was tuned to increase rotational speed from 35000 min^{-1} to 38000 min^{-1} allowing an increase to the total power output from 0,96kW to 1,17kW, although the initial values provided by the manufacturer are theoretical. These values can be found in Table 1.5.

Furthermore, the piston is casted aluminium with a 24% of silicon and a very fine grain, which increases stability when facing variable temperatures or stretching (L. Parramón, 1997).

Engine		
Model	Profi Speed	
Power	1170	W
Angular Velocity	38000	min^{-1}

Table 1.5. Engine Input Values.

2. Boundary Conditions

2.1. Speed and Flight Height

To understand flight parameters such as the speed of the model and its height, it is imperative to again take a look at the sporting code by the FAI. In the aforementioned document, it is stated that the "*flying height must not be less than one metre and not more than 3 metres*" (FAI, 2017). If these boundaries are broken during more than a lap, or a height of 6m is exceeded, the flight is cancelled and its timing considered invalid.

Speed is measured considering the total time it takes the model to fly around 9 laps of the circuit, which has a flight circle radius of 17,69m. 9 laps are equivalent to 1km of trajectory so speed (in km/h) is calculated by dividing 3600 by the total time taken in seconds. As it will be demonstrated in this study, the length of the lines can vary due to stretching and aerodynamic drag, yet nevertheless official speed for record keeping purposes is always calculated considering there are 17,69m from the centre of the circle to the model's axis of propulsion.

At the centre of the flight circle, the lines are attached to a control handle and pylon fork (Figure 2.1) which should have a height of between 1m and 1,6m. This would mean that a model flying at an altitude of 1m with a pylon adjusted to the same height, would have a true flight radius of 17,69m if the lines were considered rigid.

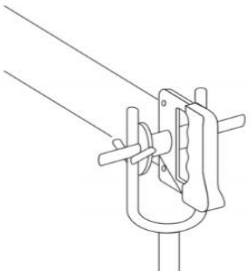

Figure 2.1. Handle Attached to the Pylon and lines. FAI.

However, since in order to cover the 9 laps of the circuit in the minimum time, it is optimal to reduce the trajectory covered, it is best to fly at the maximum permitted altitude, 3m, since this will make the flight radius smaller, and thus decrease the overall time. Likewise, if the height of the handle is at its minimum, 1m, the true flight radius is decreased even more.

To have a sense of just how much the height affects the true speed of the aircraft the following three examples can be compared side by side in Table 2.2. Example 1, flies at the minimum permitted height, but also has the handle set at the minimum height, 1m. Since both heights are the same, the model would fly with its lines parallel to the ground and the flight radius would be 17,69m. Example 2, flies with both flight height and handle height at its maximum permitted height, so the flight radius is reduced, but not as much as in Example 3, when flight height is

at its highest, and handle height is at its lowest. Figure 2.3 can help to better understand the reason behind the flight radius shortening.

	Example 1	Example 2	Example 3
Pylon and Fork Height	1000 (min)	1600 (max)	1000 (min)
Flight Height	1000 mm (min)	3000 mm (max)	3000 mm (max)
True Flight Radius	17690 mm	17617,75 mm	17576,66 mm
Time taken to complete 9 laps	12s	12s	12s
Official Speed	**300 km/h**	**300 km/h**	**300 km/h**
Real Speed	**300 km/h**	**298,77 km/h**	**298,07 km/h**

Table 2.2. How shortening the flight radius reduces time needed to complete 9 laps.

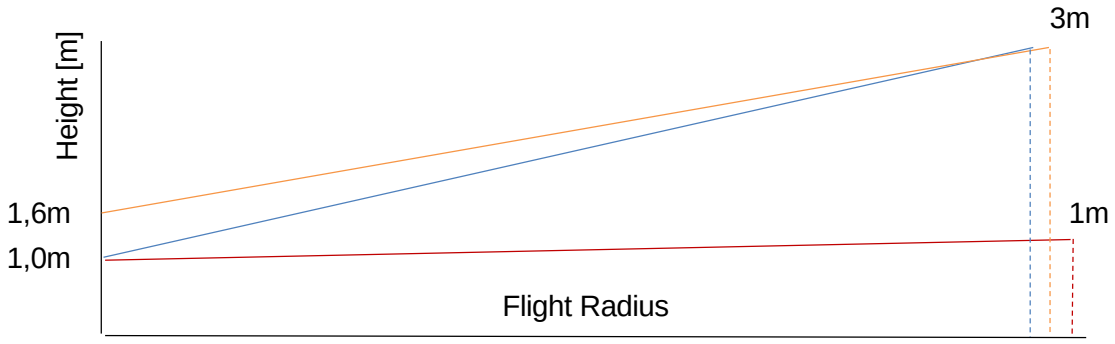

Figure 2.3 Shortening of flight radius due to difference in height. Own elaboration.

As can be observed, the only case in which the official speed would be equal to the real speed would be in example 1, and example 3 would be the one to take more advantage of the timing system, since the great difference between the pylon height and the flight height would decrease the true flight radius, and thus the model would need to travel at the lowest speed (~298 km/h) to obtain the same official speed of 300km/h.

However, the comfort of the pilot must also be taken into account, since it is not always possible to crouch down and hold the lines at a height of just 1m, which would decrease the mobility of the pilot around the pylon. For that reason, for this study, even though the maximum permitted flight height has been used (3m), the pylon height shall be that of Lluís Parramón's usual handle height: 1,4m. It is worth noting that most pilots fly with the pylon at similar values, depending on their height.

The chosen speed for this thesis will be 302,5km/h. This is the speed of one of the most recent attempts of Lluís Parramón with this model, in 2002, which is the fastest circuit time for the model at hand. However, this model had achieved speeds of 311,2 km/h when it won its first World Championship in 1996. However, back then, sporting regulations enforced the length of the wires to be of 15,92m so the overall drag of the wires was much lower. The mentioned speed and heights will be introduced in Table 2.4 in order to compute the angular velocity of the model, and its flight angle with the horizontal plane.

Performance		
Speed	302,50	km/h
Speed	84,03	m/s
Flight Height	3	m
Handle Height	1,4	m
Flight Radius	17,55	m
Angular Velocity	4,767	rad/s
Flight Angle	9,58E-02	rad
Flight Angle	5,49	degrees

Table 2.4. Performance Input Table

To calculate the angular velocity and the flight angle, the lines have been approximated to being completely straight, a theory that will be later put to the test. Like so, the flight radius has simply been approximated using Pythagoras' theorem (Eq 1.1)

$$X = \sqrt{Length\ of\ lines\ (until\ CG)^2 - (Flight\ Height - Handle\ Height)^2} \qquad (Eq\ 1.1)$$

$$Flight\ Radius = 17550\ mm$$

As a result, the flight angle can be calculated using the newfound flight radius and the difference in handle and flight height, as can be seen in Eq. 1.2.

$$Flight\ Angle = \tan^{-1}\left(\frac{Flight\ Height - Handle\ Height}{Flight\ Radius}\right) = 0{,}00958\,\text{rad} \qquad (Eq\ 1.2)$$

2.2. Atmospheric Conditions

2.2.1. Temperature and Pressure

Usually, atmospheric conditions are the variables contestants have least control over. Due to this, normal temperature and pressure conditions will be used (20 °C, 101,325 Pa) (EEA,

1999). It is also contemplated further on in the study how these conditions can affect flight performance.

These variables have the most significant effect on properties of the air such as dynamic viscosity and density, both relevant to the aerodynamic study of the model. In the Excel program, the density of air has been calculated using Eq. 2.1

$$\rho = \frac{p \cdot M}{R \cdot T} \qquad (Eq. 2.1)$$

Similarly, gas viscosity is computed using Sutherland's formula, Eq. 2.2 (Crane, 1988):

$$\mu = \mu o \cdot \left(\frac{a}{b}\right) \cdot \left(\frac{T}{To}\right)^{1.5} \qquad (Eq\ 2.2)$$

$$a = 0.555\,To + C$$
$$b = 0.555\,T + C$$

2.2.2. Wind

Since sporting regulations do not allow competitions to take place if there is a sustained wind stronger than 9m/s (32,4 km/h) for at least 30 seconds, any value below that will be considered negligible next to the airspeed of control line speed models, which may well reach over 85m/s. Thus, the resulting Table 2.5 for atmospheric conditions is as follows, and is used in elaborating Table 2.6 which contemplates the air properties mentioned.

Conditions		
Air Temperature	20,00	°C
Air Temperature	527,67	°R
Pressure	101,325	KPa
Gravity	9,81	m/s^2

Table 2.5. Atmospheric Conditions

Air		
Dynamic Viscosity	1,8369E-05	Pa s
Density	1,21	kg/m^3

Table 2.6. Air Properties

The use of a cell with the value of gravity on Earth can be useful for referencing it when calculating weights, tensions, and other forces.

3. Aerodynamic Lift

For any aircraft, model or life-size, there are usually two pairs of forces in equilibrium at the same time: Weight and Lift, and Thrust and Drag. For the case of control line, an additional pair is of strict relevance: the line tension and the centripetal force which gives the model a circular trajectory.

Since the model for this study uses a symmetrical aerofoil (NACA 0012), this profile would not create any lift force if it was not tilted at a certain angle of attack, so the first task at hand must be to find that angle, since the drag force of the wing will also depend on it.

In addition to tension, the lines are submitted to other forces such as drag and their own weight, all of which contribute to a phenomenon which is crucial to understand in order to study the behaviour of the model: the line arching.

The curvature of the cables occurs in two different directions. Firstly, the simpler direction to study is the vertical one, in which the cables form catenary arches due to their own weight. The second direction, along the plane of flight, is a product of the differential drag forces applied to the lines added to the centripetal force so its shape is much more complex to plot, as the drag force also varies along the lines. This latter curvature will be addressed when studying the drag forces involved in detail.

3.1. Catenary Arches and Required Lift

In order to calculate the lift required from the model, and thus find the angle of attack, the equations for catenary arches can result useful. Catenary curves have been studied for centuries, especially for architectural purposes. Not to be confused with a parabolic curve, a catenary curve can be obtained simply by holding a hanging rope by its two ends. The weight of the rope, together with the tension applied at the two ends will define the geometry of this catenary curve, a hyperbolic cosine. If inverted, this curve can be used as what is called a catenary arch, which has excellent architectural properties such as withstanding its own weight at the same time as redistributing thrust along its centre.

For this purpose, some catenary equations have been adapted from the NASA Glenn Research Centre (N. Hall, 2015), which were originally created to calculate the curve of the line holding a kite. Such equations can be seen in Figure 3.1. In the case of control line, the same equations will be used but replacing the drag force with the centripetal force, due to the

circular movement.

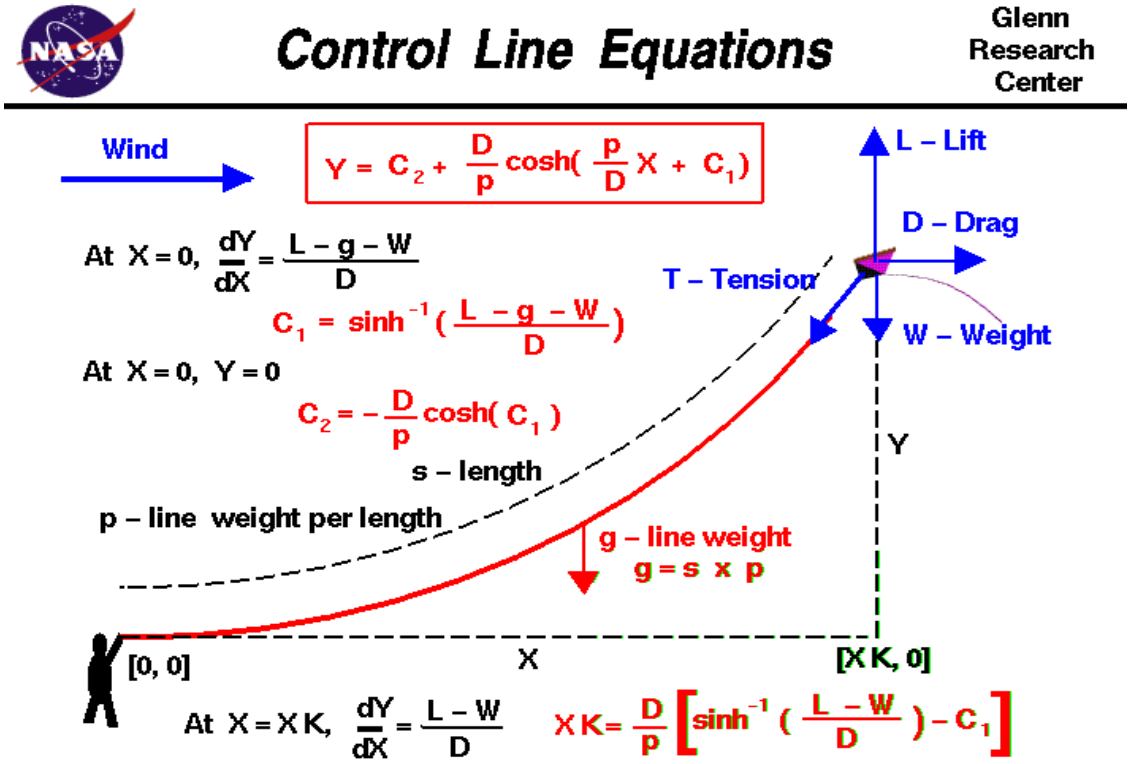

Figure 3.1. Original Catenary Equations used to calculate curvature of a kite line. NASA Glenn Research Centre. Nancy Hall.

For this study however, it not only important to substitute the forces in the previous diagram with the ones of control line, but it is also crucial to take into account that some of these forces sometimes need to be projected, as they are not applied along the vertical and horizontal axis. The following sketch will help to understand:

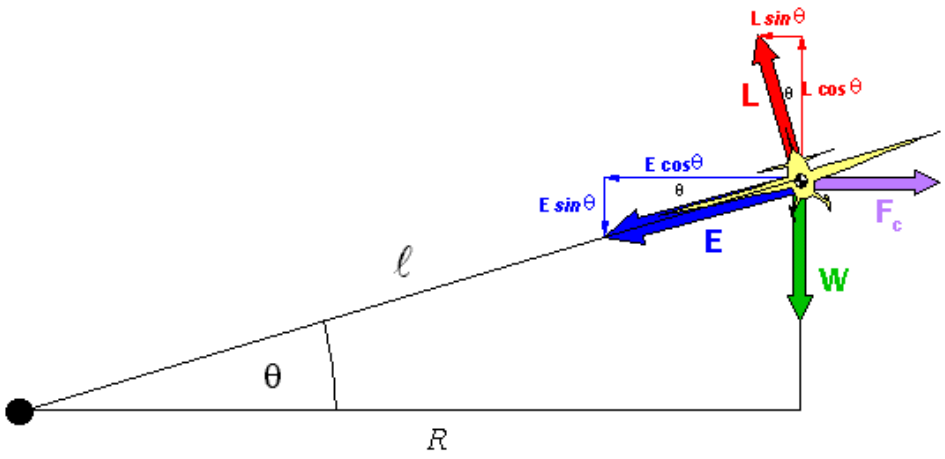

Figure 3.2 Directions of some forces involved in control line. Aerotools.de

As can be seen, weight and the centripetal force follow vertical and horizontal axis respectivly, thus the latter can be a coherently substituted for the drag of the kite model. This is also true for the tension, which, like in the NASA kite model, it also follows the direction of the lines. However, for control line, the slight inwards tilt of the aircrat creates a lift force that needs to be projected into the vertical and horizontal axis. Doing so, results in the following equations in which lift acts partly in the vertical direction, but also partly contributes to reduce the effect of the centripetal force. Eq. 3.1 is then adapted from the Glenn Research Centre equations and computes the height of the model and lines using the distance from the centre of the flight cirlce. These will be used to plot the possible catenary arch of the lines.

$$\boldsymbol{Y = C2 + \frac{Fc - Lsin\theta}{q} \cdot cosh\left(\frac{q}{Fc - Lsin\theta}\ X + C1\right)} \qquad (Eq.\,3.1)$$

$$At\ X = 0, \quad \frac{dX}{dY} = \frac{Lcos\theta - p - W}{Fc - Lsin\theta}$$

$$\hookrightarrow \quad \boldsymbol{C1 = \sinh^{-1}\left(\frac{Lcos\theta - p - W}{Fc - Lsin\theta}\right)}$$

$$At\ X = 0\ and\ Y = 0$$

$$\hookrightarrow \quad \boldsymbol{C2 = -\frac{Fc - Lsin\theta}{q}\ cosh(C1)}$$

By plotting Eq 3.1, since the lift force is the only unknown variable, it can be iteratively modified in order to obtain a desired height at the end of the lines, 3m, the flight height of the model. Simple iteration is possible thanks to the Excel program which includes all of the formulae above, then it is just necessary to change the values of lift until the desired height has been obtained.

All of the forces except for lift are known, and can be found as follows. Note that mass is the property of the control line model, not the lines.

$$\boldsymbol{Weight\ (W)} = Mass \cdot Gravity = 0{,}43 \cdot 9{,}81 = 4{,}12\ N \qquad (Eq.\,3.2)$$

$$\textbf{Centripetal Force } (F_c) = \frac{Mass \cdot Speed^2}{Line\ Lenght\ (Until\ CG)} = \qquad (Eq.3.3)$$

$$= \frac{0{,}42 \cdot 84{,}14^2}{17{,}627} = 169{,}38\ N$$

$$\textbf{Line Load } (T) = Mass \left(\frac{Speed^2}{Line\ Lenght\ (Until\ CG)} - Gravity \cdot \sin(flight\ angle) \right) = \qquad (Eq.3.4)$$

$$= 0{,}57\ \frac{84{,}14^2}{17{,}627} - 9{,}81 \cdot \sin(0{,}18) = 167{,}84\ N$$

$$\textbf{Distributed weight of the line } (q) = \frac{Line\ Weight}{Line\ Length\ (until\ wing)} = \qquad (Eq.3.5)$$

$$= \frac{0{,}0164}{16{,}73} = 9{,}62 \cdot 10^{-3} N/m$$

Next, the following values have been used in Table 3.3 at the same time as modified lift, and it has been found that a lift of 29,06N is required to obtain a flight height of 3m.

W - Weight	4,1202	N
Fc - Centripetal Force	168,93	N
L - Lift	**29,06**	N
T - Line Tension	167,84	N
Constant - C1	0,09374	
Constant - C2	-17349,66	

Table 3.3. Values obtained for the different forces involved in the catenary curve.

Distance from centre (mm)	Height (m)
0	1,50
1000	1,59
2000	1,68
3000	1,76
4000	1,85
5000	1,94
6000	2,03
700	2,12
8000	2,20
9000	2,29
10000	2,38
11000	2,47
12000	2,56
13000	2,65
14000	2,73
15000	2,82
16000	2,91
17000	**3,0000**

Table 3.4 Height of the model versus x

If we plot the values of Table 3.4, Figure 3.5 is obtained:

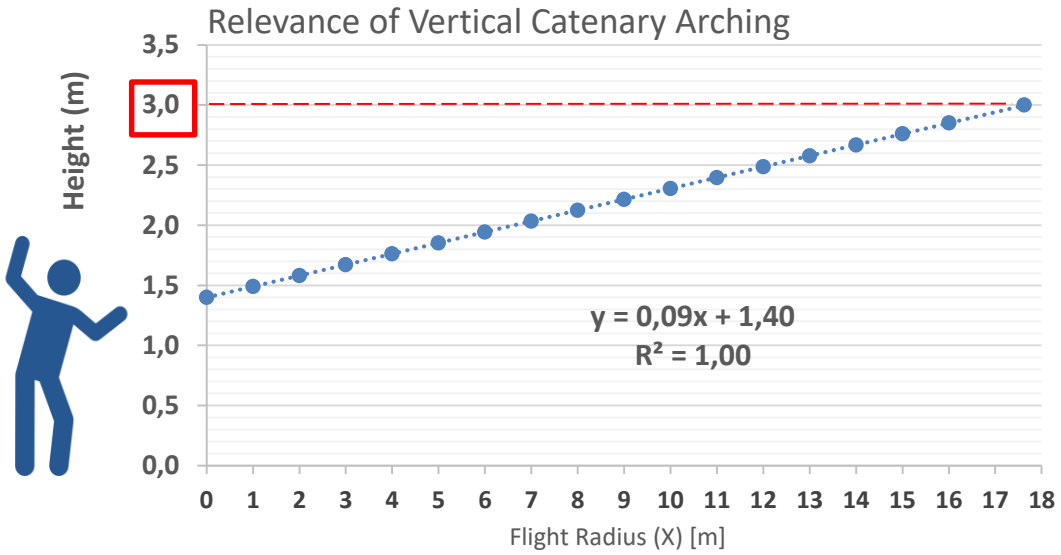

Figure 3.5. Flight height versus distance from center of flight. Own elaboration.

As it can be observed, the catenary curvature along the vertical axis, the direction of the lines' weight, is negligible. One might doubt these results since there is a perfect correlation in the linear regression ($R^2 = 1$), but this is due to the insignificance of the weight of the wires (1,6N in total), next to the centripetal force (169N). To further defend this hypothesis and validity of the calculations, an example with much longer lines has been carried out in Figure 3.6, to show how long these would need to be in order for a curvature to be noticeable.

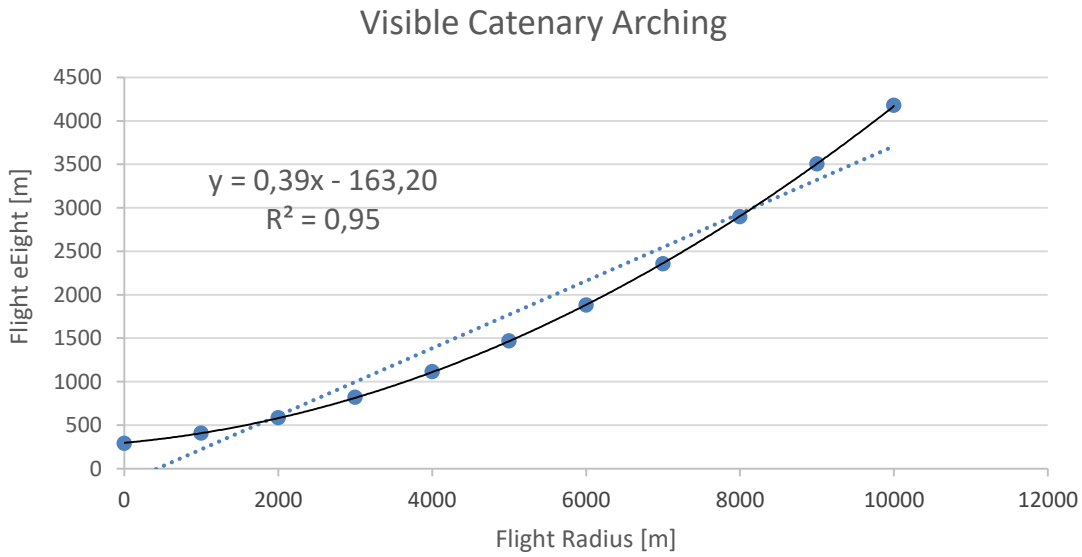

Figure 3.6. Flight height versus distance from center of flight on much longer lines.

Indeed, the lines would have to be more than 500 times longer for the curvature to be noticeable.

Having demonstrated that the vertical catenary curve is negligible, the height of the model along its radius will from now on be treated as a linear dependency. In Annex A.1, a graph has been plotted, this time to scale, in order to better understand the dimensions and forces involved.

Figure A.1 has been plotted to scale once linearity has been proven. It shows the four forces at balance on the vertical plane, and the aproximate distance from the person flying the model and the latter.

3.2. Finding the angle of attack once the Lift force has been calculated

Thus, in order to obtain an exact flight height of 3m, the required lift can be found by iterating values of lift until the desired height is obtained and it results in 29,06N for this study. As previously stated, due to the symmetrical profiles of both the wing and the stabilizer, this lift is a result of the angle of attack of the model.

So in order to calculate this angle of attack, the lift force found needs to be introduced in Eq. 3.6, to find the lift coefficient, which is unique to a specific angle of attack for the profile in this study, and a concrete Reynolds number.

$$Cl = \frac{Lift}{\frac{1}{2} \cdot Air\ Density \cdot Speed^2 \cdot A_T} \qquad (Eq\ 3.6)$$

The total projected area of the wing and stabilizer is computed in the *Input* tab of the Excel worksheet, approximating the geometry of both parts to trapezoids. Therefore, it is only necessary to know the length of the cord at the tip and at the base of each part, and its length. The total area will be calculated using Eq 3.8, a simple adaptation from the trapezoid area formula (Eq. 3.7).

$$Area = \frac{(a+b) \cdot h}{2} \qquad (Eq. 3.7)$$

$$Area = \frac{(Chord\ at\ tip + Chord\ at\ base) \cdot Length}{2} \qquad Eq.3.8$$

For the wing:

$$Area = \frac{(18mm + 60mm)\ 935mm}{2} = 36465mm^2 = 0{,}036\ m^2$$

For the Stabilizer:

$$Area = \frac{(55mm + 90mm)\ 170mm}{2} = 12325mm^2 = 0{,}012\ m^2$$

Hence, the total area of the wing and stabilizer can be added up:

$$A_T = 3{,}65 \cdot 10^{-2} + 1{,}23 \cdot 10^{-2} = 4{,}88 \cdot 10^{-2}\ m^2$$

Air density will be computed in the Excel program under normal conditions, and speed will be approximated to 300 km/h as the speeds from the tip of the wing to the tip of the stabilizer range from 287 to 306 km/h respectively. Then, the lift coefficient required can be calculated from the lift formula (Eq. 3.6) and the resulting lift coefficient is therefore 0,1423.

$$Cl = \frac{29{,}06}{\frac{1}{2} \cdot 1{,}21 \cdot \left(\frac{300}{3{,}6}\right)^2 \cdot 0{,}00488} = 0{,}1423$$

For the profile in this study, a NACA 0012, if experimental plots are consulted on airfoiltools.com, one of the biggest sources of information about aerofoils, various graphs relating lift coefficients and angles of attack can be found, depending on the Reynolds number. The intervals of numbers are quite wide, (the closest values for this study would be either Re = 200 000 or Re = 500 000, but it has been observed that values of the angle of attack for such low lift coefficients don't vary significantly, so the closest value to this case, Re = 200 000, will be used.

As can be observed in Figure 3.1 there is a part of the graph that closely resembles a linear tendency, from an angle of attack of 10° to -10°. This range will be used to compute a regression line that will give an estimate of the required angle of attack to obtain a certain Lift coefficient.

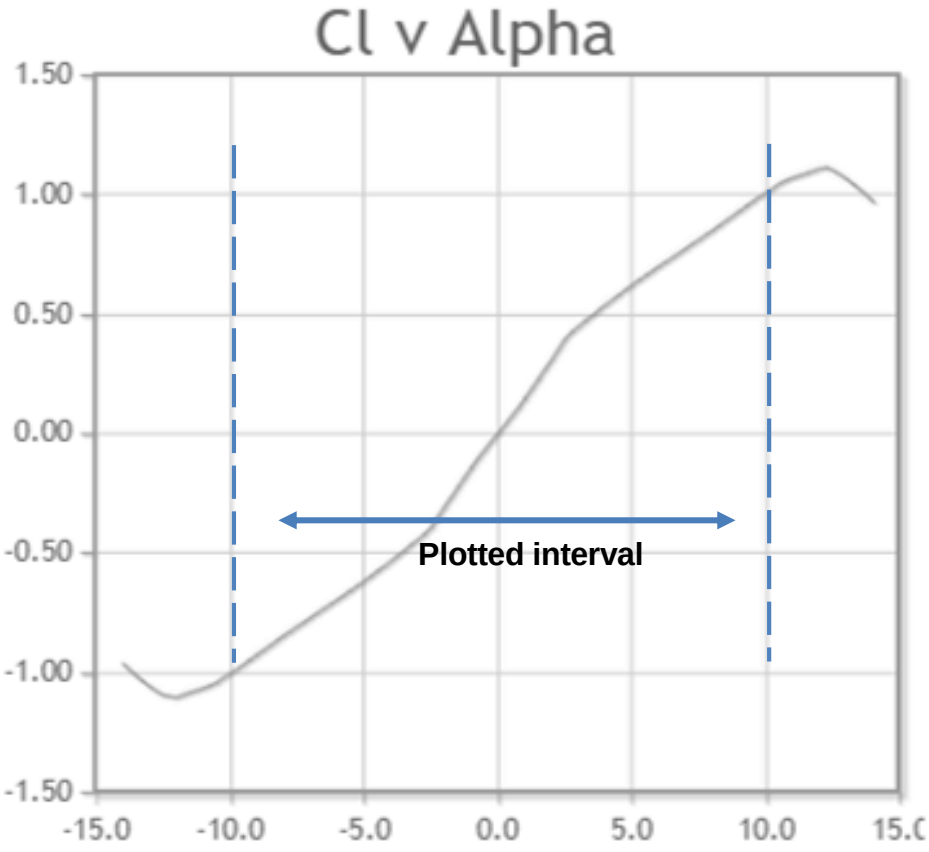

Figure 3.7 Lift Coefficient evolution with angle of attack. Airfoiltools.com

For this concrete case however, only positive angles of attack are relevant, as positive lift is required to keep the model in the air. Despite this, the regression line will take into account positive and negative values of the angle in order to improve accuracy.

As can be observed in Graph 3.8, the linear regression crosses the origin of the coordinate system, as there is no lift created from a non-existent angle of attack (symmetrical aerofoil).

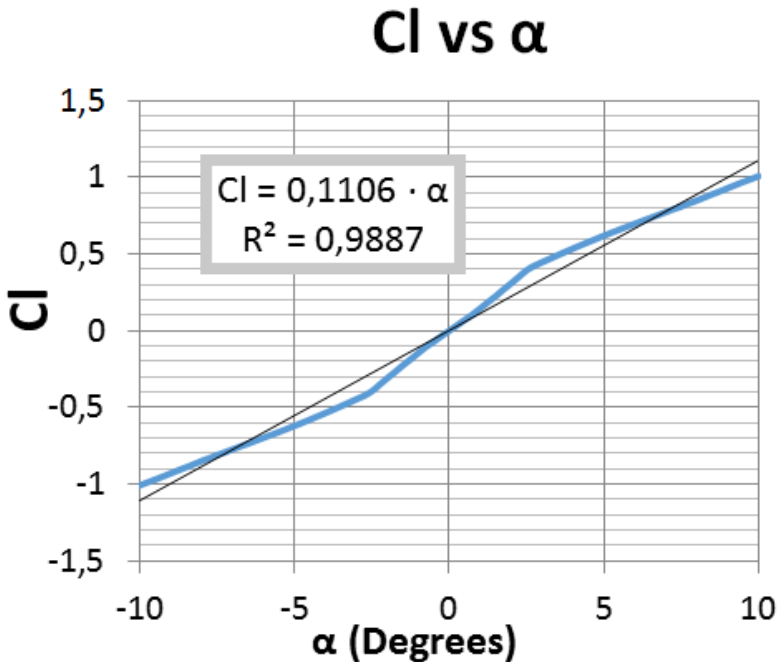

Graph 3.8. Linear Regression of Cl vs α. Own Elaboration

There is a very strong linear tendency (R^2 = 0,9887) so the resulting formula (Eq 3.7) will be used to calculate the angle of attack for the previously calculated lift coefficient (0,1452).

$$\alpha = \frac{Cl}{0{,}1106} = \frac{0{,}1423}{0{,}1106} = 1{,}29° \qquad (Eq\ 3.7)$$

Thus, the model in this study is required to fly at a very small angle of attack, of only 1,28°. This angle could of course cause an error in calculating the projected area of the wing and stabilizer, but as can be seen in Eq. 3.8, this error is negligible and so this angle will not be taken into account when calculating projected areas.

$$error\ (\%) = \frac{True\ Projected\ Area - Aproximated\ Projected\ Area}{True\ Projected\ Area} \cdot 100 = \qquad (Eq.3.18)$$

$$\frac{4{,}73 \cdot 10^{-2} \cdot \cos\left(1{,}29\frac{2\pi}{360}\right) - 4{,}73 \cdot 10^{-2}}{4{,}73 \cdot 10^{-2} \cdot \cos\left(1{,}29\frac{2\pi}{360}\right)} \cdot 100 = 0{,}0012\%$$

And so, in the excel worksheet a table can be found under the *Lift* tab that summarizes the results of the calculations for finding out the angle of attack, which will be the end of this particular tab of the worksheet.

Lift	**29,06**	N
Wing Surface Area	**3,65E-02**	m^2
Stabilizer Surface Area	**1,23E-02**	m^2
Total Area	**4,88E-02**	m^2
Cl for Required Lift	**0,14229**	
Angle of attack	**1,29**	°
Error in projected area	**0,0012**	**%**

Table 3.13. Output of the lift calculations and angle of attack.

This concludes the calculations involving lift force of the model, so now the other important aerodynamic force remains, drag.

4. Aerodynamic Drag

4.1. Model Drag

Perhaps one of the most influential forces the model is submitted to, and the one that pilots try to minimize in order to gain speed, is aerodynamic drag. One might think that due to the small section of the wires, most of the resulting drag would come from the model, with a greater frontal area, and traveling at much higher speeds than the rest of the cable. One would indeed be very wrong.

As it will be demonstrated, the length of the control lines is so great that its drag actually makes up for most of the total drag of this study. In order to study the drag accordingly, the model will be divided into sections with slightly different behaviour, these are: the lines, the wing, the fuselage and the stabilizer. For most of the sections, an equation relating the differential drag force with the distance from the centre of the flight centre will be found. The only exception will be drag force of the fuselage, since the area taken into account for calculating this force is the total frontal projected area, the drag will be calculated as a whole. A representation of the different segments can be found below, in Figure 4.1.

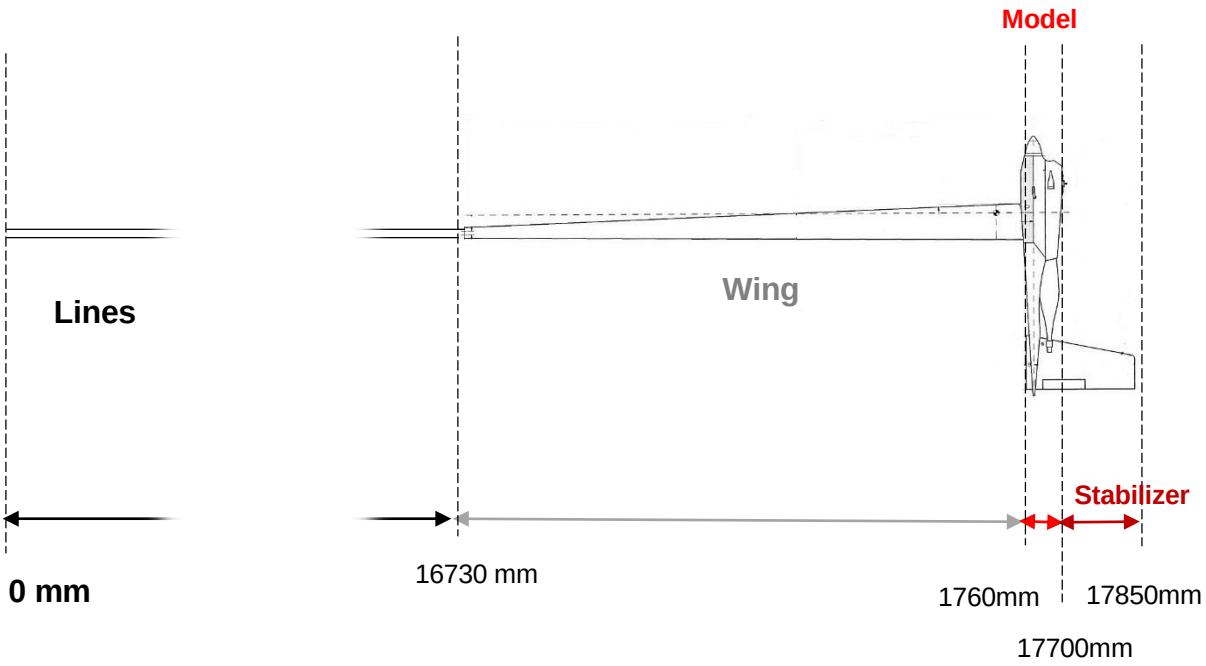

Figure 4.1. Different sections in which drag will be studied. Own Elaboration

4.1.1. Lines

As mentioned before, the aerodynamic drag of the lines will be of the greatest importance, due to its total value. In order to calculate such value, the lines will be divided into sections, with the hope to find an equation that relates the differential drag force of each section with the distance from the centre of flight radius, and then integrate this equation to obtain the total drag. For this particular study, the lines have been divided into segments that are 1000mm apart, except at the start and end of the lines, where the behaviour might vary slightly, so less distance is taken. For each of these sections, differential drag has been calculated as follows:

For the drag equation:

$$D = \frac{1}{2} \cdot Cd \cdot Air\ Density \cdot Speed^2 \cdot Area \quad [N] \qquad (Eq.\ 4.1)$$

Where *Area* (total area) would in fact be the frontal area of the lines (diameter), times the length of these and the number of lines. So if we want to find the differential drag of each section, Eq. 4.2 must be used (Column I (Drag (N/m) of the *Drag* tab of the worksheet):

$$\frac{D}{L} = Cd \cdot \frac{1}{2} \cdot Air\ Density \cdot Speed^2 \cdot number\ of\ lines \cdot Diametre \left[\frac{N}{m}\right] \qquad (Eq.\ 4.2)$$

Now, out of these variables, air density, the number of lines and their diameter are constant for this study. Speed, can be easily calculated with the angular velocity of the model, computed in the Input tab, simply multiplying by the distance from the centre of the flight circle.

Perhaps the most complex variable to study is the drag coefficient (Cd). Like most aerodynamic coefficients, it depends on the Reynolds number value for each section, which in turn depends on speed, dynamic viscosity of the air, air density and a characteristic length. For the case at hand, the characteristic length of a wire is its diameter. However, even if the Reynolds number for each section is calculated, the dependency between this number and its drag coefficient is not linear, nor in fact can easily be characterised mathematically. For this reason, many studies which try to tackle such problem (P. Soule 1972), end up giving an approximate drag coefficient to be used along all of the sections (usually around 0,95).

This study will try to use experimental data to improve accuracy when calculating drag coefficients that depend on the Reynolds number, so Graph 4.3 has been used, from a study by P. Soule (1972).

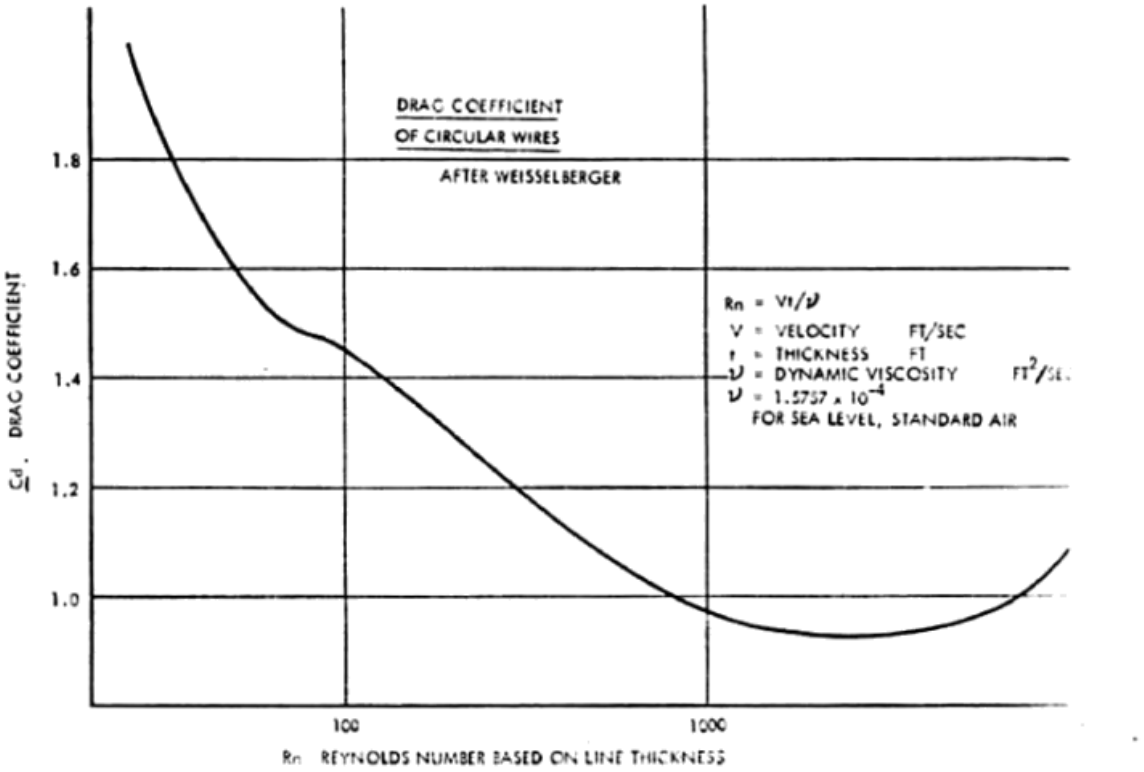

Graph 4.2. Experimental Data of Drag Coefficient Values versus Reynolds Numbers for ciruclar wires. P. Soule.

This graph plots experimental drag coefficient data versus Reynolds numbers for circular wires, and it can be observed that despite the initial appearance of a strong parabolic dependency, the logarithmic scale of the Reynolds axis makes this assimilation untrue.

For this reason, this graph has been studied in three different Reynolds ranges, from 30 < Re < 100, from 100 < Re <1000 and from 1000 < Re < 3000. Next, using the Excel worksheet, the experimental values of the graph have been reproduced as accurately as possible, so the following graph (Fig. 4.3) is obtained:

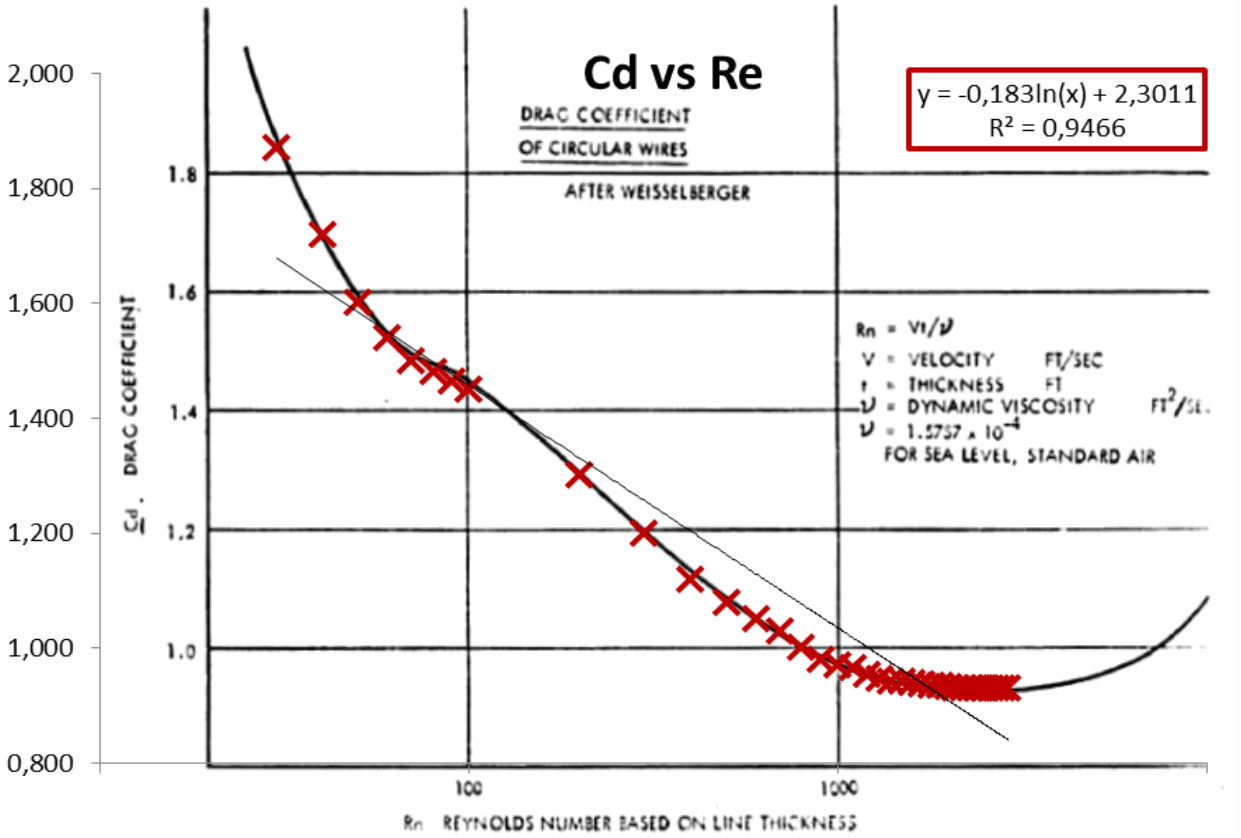

Figure 4.3. Superposition of P. Soule's Experimental Data and values created to obtain an equivalent graph.

As can be obersevd, if a first logarithmic regression is computed, the R^2 value is 0,95, which might not seem so bad at first, however, the importance of being accurate for the sections closest to the model, calls for a more precise aproximation. To have a sense of how important this is, the study mentioned (P. Soule 1972), stated that 93.8% of line drag comes from the last half of the wires and 68.3% comes from the last quarter, thus the importance of studying this dependency by sections. The graph obtained from Figure 4.3 has been further divided into three sections, depending on the Reynolds number. Thus, graphs 4.4 to 4.6 are obtained. Then a regression function is calculated using the Excel program depending on which mathematical function results in the best fit.

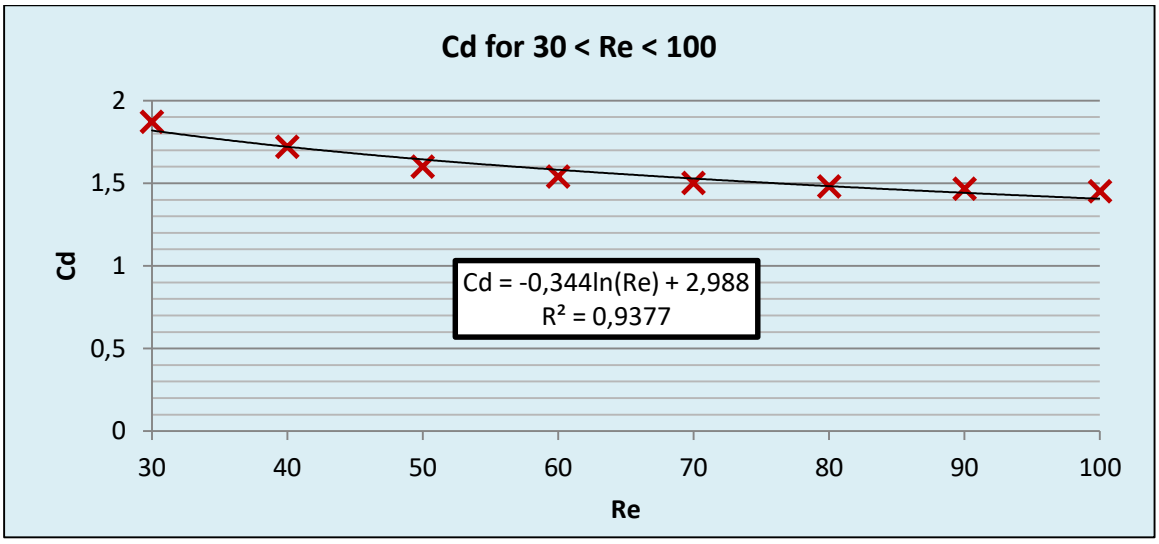

Graph 4.4. Cd vs Re Number for 30 < Re < 100. Own elaboration.

As can be seen, for the first regression interval, the R^2 value has indeed decreased, despite using the most fitting regression, a logarithmic one. However, due to the small values of speed for these Reynolds numbers, the total drag of this section is negligible.

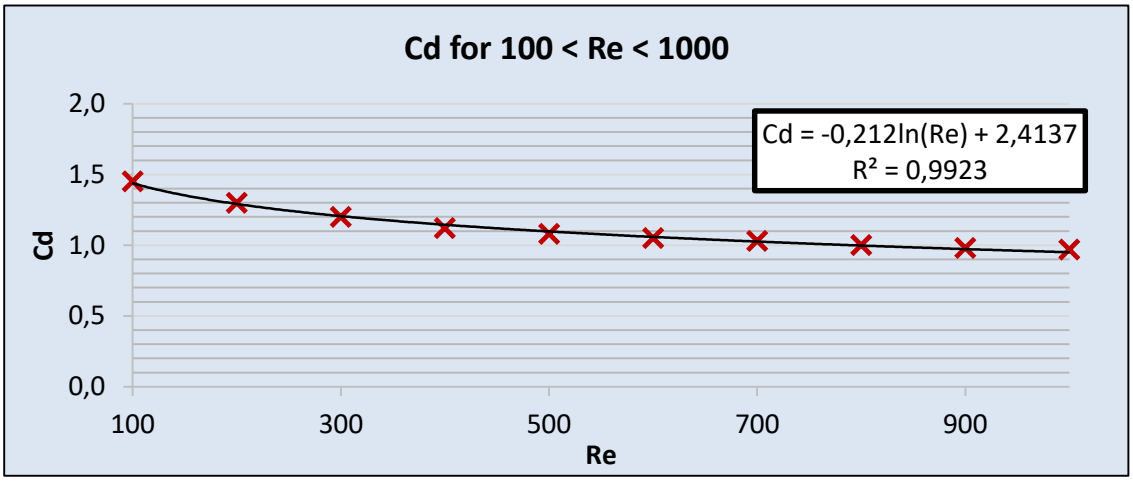

Graph 4.5. Cd vs Re Number for 100 < Re < 1000. Own elaboration.

For the second regression interval, a logarithmic expression fits almost perfectly to the experimental data, so it is safe to say accuracy has been greatly increased for this interval, which is already relevant as speeds are increasing.

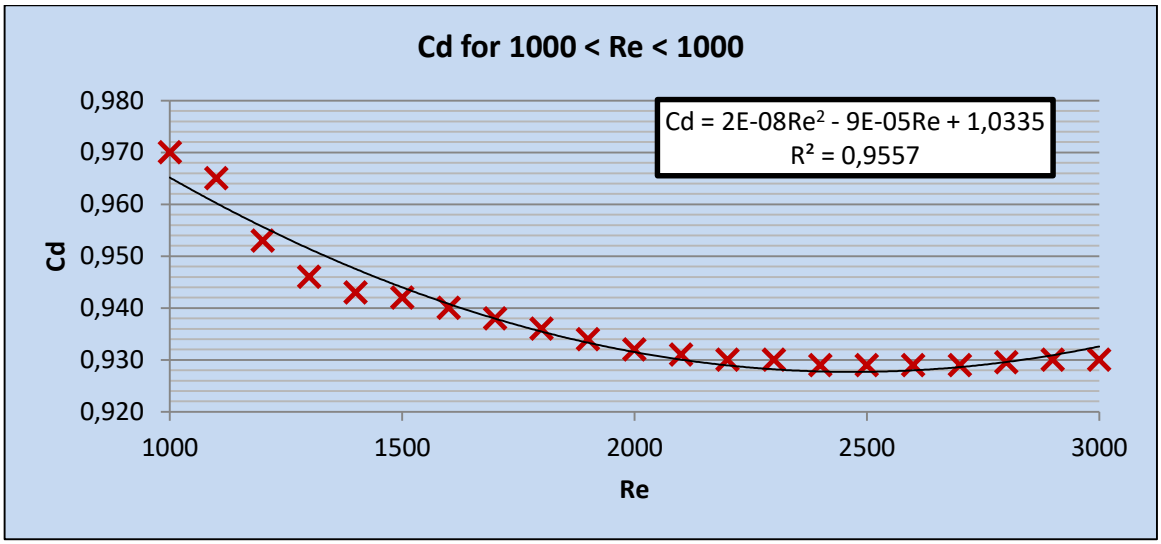

Graph 4.6. Cd vs Re Number for 1000 < Re < 3000. Own elaboration.

For the last interval, the closest to the wing and the most crucial one, as it is where most of the drag will be induced, a logarthmic equation is no longer the best fit. For this case, due to the shape of the experimental data, a parabolic expression has been found to be the closest fit, increasing the R^2 value to 0,9557.

Using the three expressions found, the drag coeffieints can now be more accurately calculated for the three sections above. This results in the following rows of the Excel worksheet, under the *Drag* tab.

Part	Radius (m)	Airspeed (km/h)	Characteristic Length	Value (mm)	Re	Cd	Drag (N/m)
Lines	0,50	8,58	Diameter	0,4	6,26E+01	1,54	0,00
Lines	1,00	17,16	Diameter	0,4	1,25E+02	1,39	0,02
Lines	2,00	34,32	Diameter	0,4	2,50E+02	1,24	0,06
Lines	3,00	51,48	Diameter	0,4	3,75E+02	1,16	0,13
Lines	4,00	68,64	Diameter	0,4	5,01E+02	1,10	0,21
Lines	5,00	85,81	Diameter	0,4	6,26E+02	1,05	0,32
Lines	6,00	102,97	Diameter	0,4	7,51E+02	1,01	0,44
Lines	7,00	120,13	Diameter	0,4	8,76E+02	0,98	0,58
Lines	8,00	137,29	Diameter	0,4	1,00E+03	0,99	0,77
Lines	9,00	154,45	Diameter	0,4	1,13E+03	0,99	0,97
Lines	10,00	171,61	Diameter	0,4	1,25E+03	0,98	1,19
Lines	11,00	188,77	Diameter	0,4	1,38E+03	0,97	1,42
Lines	12,00	205,93	Diameter	0,4	1,50E+03	0,96	1,68
Lines	13,00	223,10	Diameter	0,4	1,63E+03	0,95	1,95
Lines	14,00	240,26	Diameter	0,4	1,75E+03	0,94	2,23
Lines	15,00	257,42	Diameter	0,4	1,88E+03	0,93	2,53
Lines	16,00	274,58	Diameter	0,4	2,00E+03	0,91	2,84
Lines	16,73	287,11	Diameter	0,4	2,09E+03	0,90	3,08

Table 4.7. Data used to calculate differential drag along the lines.

In order to calculate the total drag of the wires using integration methods, an equation that related the radius from the centre of flight to the differential drag must be found, in order to integrate along the radius. If the corresponding columns are plotted (Radius and Drag of Table 4.3), the following graph is obtained:

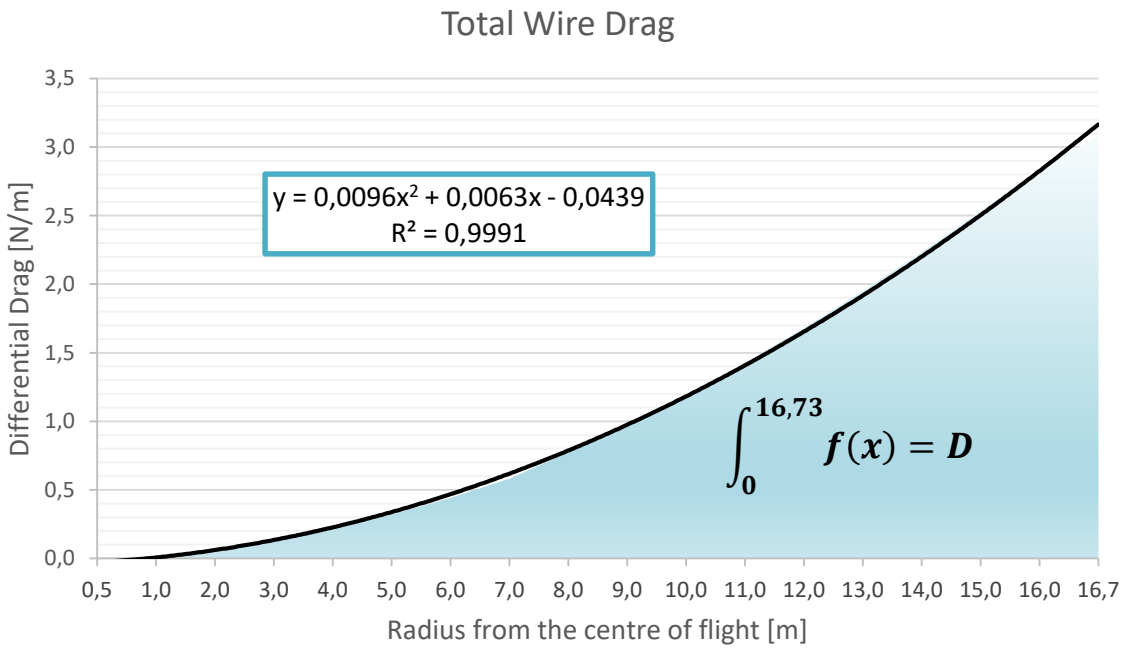

Graph 4.8. Equation and area used to find the drag force of the lines

As can be observed, a second degree polynomial fits very well, due to the strong dependency of speed, which is squared in the drag equation. Thus, the blue area, the total drag, can be found integrating the parabolic equation, as shown in Eq 4.4.

$$\int_0^{16,73} 0,0096x^2 + 0,0063x - 0,0439 = \mathbf{15,14N} = Total\ Wire\ Drag \qquad (Eq\ 4.4)$$

After calculating the rest of the drag forces for each part of the model, the error in calculating the previous drag if a constand value for Cd had been used, will be shown.

4.1.2. Wing

As for the wing, its aerofoil is a NACA 0012, a symmetrical profile which does not provide any lift force if it is not tilted at a certain angle of attack. However, the symmetry of the profile also allows the wing to reduce its drag considerably.

To study the drag force along the wing, Eq 4.5 for calculating drag force will be used:

$$D = Cd \cdot \frac{1}{2} \cdot Air\ Density \cdot Speed^2 \cdot C \cdot L \quad [N] \qquad (Eq. 4.5)$$

Where instead of using the total area of the wing (A), its length times its chord has to be used, the latter varying along the flight radius. This allows calculating the differential force instead of the total force acting on the wing using Eq 4.6.

$$\frac{D}{L} = Cd \cdot \frac{1}{2} \cdot Air\ Density \cdot Speed^2 \cdot C \quad \left[\frac{N}{m}\right] \qquad (Eq. 4.6)$$

The wing has been divided into 10 more or less equally distributed segments, and calculating the differential drag force of each one can be used to obtain a polynomial equation which when integrated can result in the total drag force of the wing, similarly to the process carried out for the wires. Since each parameter varies differently along the radius, here is how each one is calculated:

Drag Coefficient: Constant for the previously calculated angle of attack of 1,29°: 0,0104. Information relating each angle of attack with drag coefficient can be found at airfoiltools.com, similarly to how it was found for the lift coefficient

Air Density: Constant for the standard conditions of this study: 1,21 kg/m^3

Speed (or Airspeed): Calculated with the angular velocity of the model and the distance from each segment to the centre of the flight radius ($Speed = \omega \cdot x$)

Chord: Since the only known values of the chord for the wing are those at the tip and at the wing base, the assumption that the chord varies linearly between the two has been made, and thus another linear equation (Eq 4.7) relating chord and radius can be found.

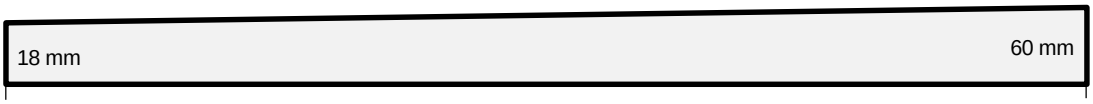

16730 mm $Chord = 44{,}33 \cdot x - 723{,}59$ $(Eq.4.7)$ 17680 mm

$$for\ 16730\ mm < x < 17680\ mm$$

So if all parameters are calculated, for all 10 segments, Table 4.9 can be obtained which relates distance from the centre (x) and differential drag (D/x) which can then be plotted in Graph 4.10 showing the area accountable for the total drag of the wing.

x [m]	D/x [N/m]
16,7300	0,72
16,8000	0,85
16,9000	1,04
17,0000	1,24
17,1000	1,44
17,2000	1,64
17,3000	1,85
17,4000	2,06
17,5000	2,28
17,6270	2,56
17,6775	2,68

Table 4.9

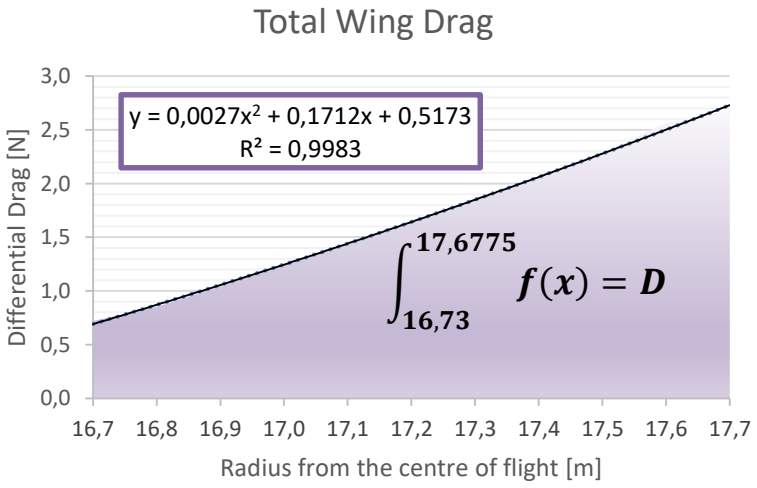

Graph 4.10. Equation and area used to compute wing drag

As can be observed, the fit is very close to perfect (R^2 = 0,9983) if a second order polynomial equation is used in the regression; and this makes sense, because drag is dependent of speed squared, which in turn, is linearly dependent of the flight radius. Due to the accuracy of this regression, the equation found will again be integrated over the length of the wing (Eq 4.8) in order to find the total drag acting on the wing.

$$D = \int_{16{,}73}^{17{,}6775} 0{,}0027x^2 - 0{,}1712x + 0{,}5173 = \mathbf{4{,}05\ N} = Total\ Wing\ Drag \quad (Eq\ 4.8)$$

4.1.3. Stabilizer

A similar approach will be used to calculate the drag of the stabilizer. Since this also uses the same aerofoil, and the quadratic dependency has already been demonstrated, fewer segments will be needed for this case, since the second degree equation will still result in an accurate fit.

In this case, the equation that relates chord and distance from the centre is Eq. 4.9:

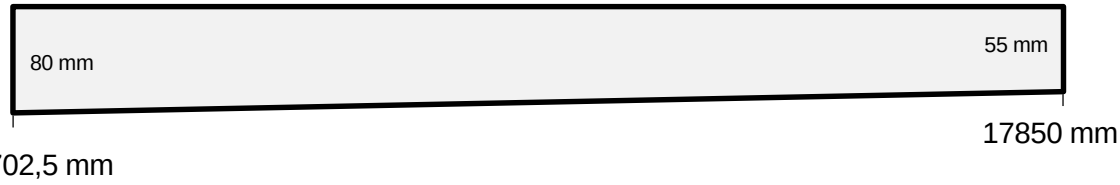

$$C = -169{,}49 \cdot x + 3080{,}42 \quad for\ 17{,}7025 < x < 17{,}85 \qquad (Eq\ 4.9)$$

Note that now the chord decreases as the distance from the centre increases, and thus drag will be smaller the further away it is from the centre even though speed is increasing with a quadratic dependency. This results in Table 4.11 and Graph 4.12.

x [m]	D/x [N/m]
17,7025	3,58
17,7500	3,24
17,8000	2,87
17,8500	2,50

Table 4.11

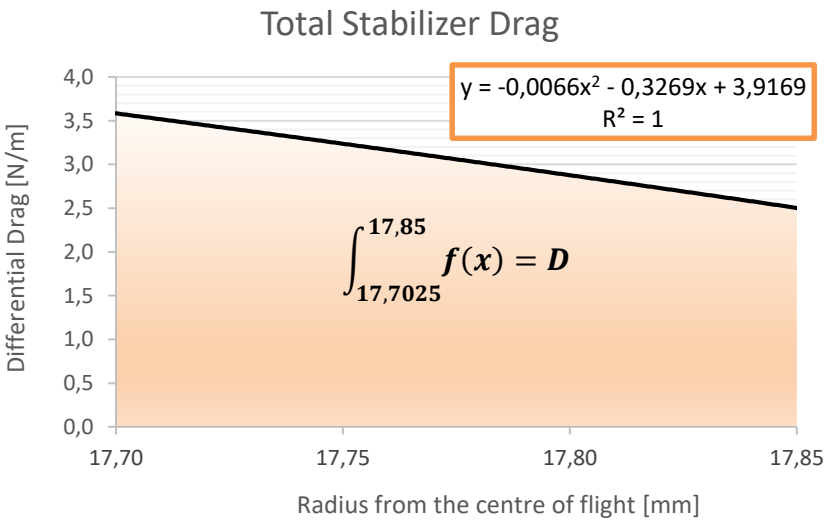

Graph 4.12. Equation and area used to compute stabilizer drag

Once again, integrating the obtained second degree polynomial, the total drag acting on the stabilizer can be found using equation 4.10.

$$D = \int_{17,7025}^{17,85} -0{,}0066x^2 - 0{,}3269x + 3{,}9169 = \mathbf{0,59\ N} = Total\ Stabilizer\ Drag \quad (Eq.4.10)$$

4.1.4. Fuselage Drag

Lastly, the fuselage's drag will be calculated in a simpler way, using the total frontal area of the model and a constant drag coefficient, which was experimentally found to be of 0,35. This was done in the wind tunnel of the ETSEIB faculty, at the Polytechnic University of Catalonia, under a previous project regarding control line flying by Salvador Gonzalez (1976).

Also, as the speed from one side of the fuselage to the other doesn't vary significantly, the average speed will be used, of 303,58km/h. And thus, the total drag of the fuselage can be calculated using Eq. 4.11

$$D = Cd \cdot \frac{1}{2} \cdot Air\ Density \cdot Speed^2 \cdot Frontal\ Area \quad [N] \qquad (Eq.4.11)$$

$$D = 0{,}35 \cdot \frac{1}{2} \cdot \frac{1{,}21kg}{m^3} \cdot \left(\frac{84{,}327m}{s}\right)^2 \cdot 2{,}3 \cdot 10^{-2}\ m^2 = \mathbf{3,46\ N}$$

4.1.5. Drag Distribution

Now that all of the acting drag forces have been found, the graph found in the annex (A.2) can help to have a sense of what is happening as the distance from the centre varies. Even though this distance is not to scale (the lines would take up too much space of the graph), it allows for a better understanding of how drag evolves along each studied section.

4.1.6. Centre of Pressure

The previously plotted drag forces, can be transformed into their equivalent point loads, or in other words, the centre of pressure of drag along each part can be found by using Eq. 4.12 (N. Hall, 2015). This is only possible because the equations relating drag force with the radius from the centre of flight have been found (Eq 4.4, 4.8 and 4.10), since they need to be integrated once more.

$$Center\ of\ pressure = \frac{\int_{x1}^{x2} x \cdot D(x)}{\int_{x1}^{x2} D(x)} = \frac{\int_{x1}^{x2} x \cdot D(x)}{Total\ Drag\ of\ Section} \qquad (Eq\ 4.12)$$

If Eq 4.12 is applied for the three sections in which a drag equation has been found (lines, wing and stabilizer), the centre or pressure of these can be found. For the fuselage, the centre of pressure will be considered in the axis of thrust, due to the approximation of a symmetrical part, with reduced dimensions and smaller speed ranges.

Therefore, a representation of the drag forces acting on their equivalent point loads (Table 4.13) would be that of Graph 4.14.

Pressure Centres (x)		
Lines	12662	mm
Wing	17158	mm
Fuselage	17690	mm
Stabilizer	17765	mm

Table 4.13. Pressure Centres for each drag force

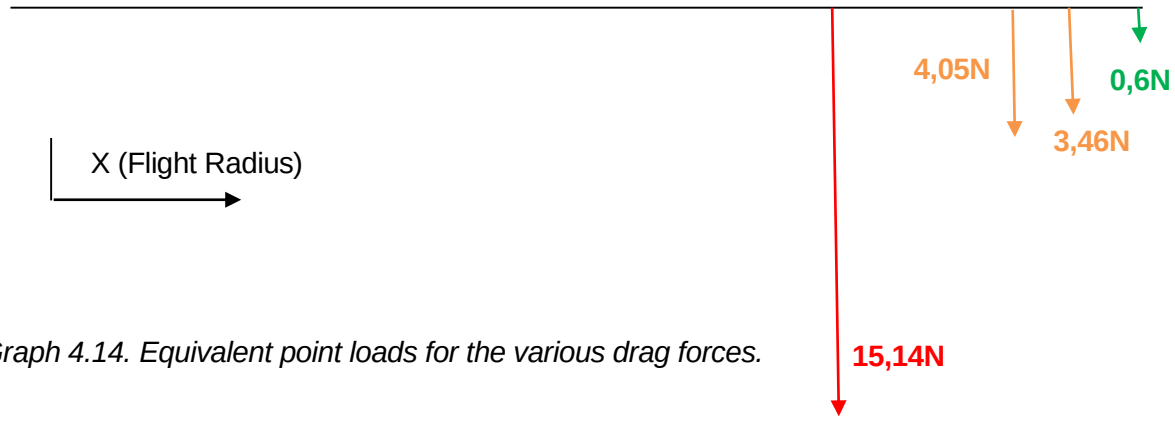

Graph 4.14. Equivalent point loads for the various drag forces.

As predicted, most of the drag (65%) is produced by the lines, even though it is the section that travels the slowest regarding airspeed. Due to its importance, line drag will be studied in depth further on in this chapter.

4.2. Power

Before studying line drag in depth, which will become more complicated than predicted, the previously calculated point loads for all the drag forces can be used to calculate the efficiency of the engine. It is important to understand that thrust provided by the engine is used entirely to counter drag force. Since they are opposing forces acting more or less in the same direction (along the plane of flight), the engine power needed can be calculated using Eq.4.13:

$$Flight\ Power = Drag\ Force \cdot Speed \qquad (Eq\ 4.13)$$

Since the drag forces have been previously simplified to point loads, the force in these points times their speed will be used to compute the total power required. As shown in Table 4.14, found under the *Power* tab of the Excel worksheet.

Drag Force	Value		Force Applied at		Speed		Power	
Supported Line Drag	**11,36**	N	12662	mm	**60,36**	m/s	**685,38**	W
Wing Drag	**4,05**	N	**17158**	mm	**81,79**	m/s	**331,26**	W
Fuselage Drag	**3,46**	N	**17690**	mm	**84,33**	m/s	**291,78**	W
Stabilizer Drag	**0,59**	N	**17765**	mm	**84,69**	m/s	**49,96**	W
Total Required Power							**1358,38**	**W**

Table 4.14. Calculation of power required to drag each part

As has been stated throughout the thesis, most of the power required from the engine goes to compensating for the large amount of drag generated by the lines. If the total power is added up, a value of 1358W is found, which is actually well above the theoretical value of power output provided by the Profi engine manufacturer, 1170W.

4.3. Line Drag

Previously, line drag has been calculated integrated using the differential drag formula (Eq 4.2) along the length of the lines. This also showed how drag evolved along the flight radius. If however, only the final value of the total drag force was of interest, total line drag could be calculated using P. Soule's approach (1972).

Considering the drag equation for wires (Eq 4.2), if speed is substituted for its value depending on the radius, taking into account the constant angular velocity, one can find the total drag (Eq 4.14) using integration since the only variable will be the radius from the flight centre (x).

$$D = n\int_{x=0}^{x=R} C_D \cdot Diametre \cdot \frac{\rho}{2}\left(\frac{v \cdot x}{R}\right)^2 dx = C_D \frac{n \cdot Diametre \cdot R}{3}\frac{\rho}{2} \cdot v^2 \qquad Eq\ (4.14)$$

In other words, if the drag calculation uses the model speed, the effective frontal area of the cables is one third of the total projected frontal area. However, Eq 4.14 does not account for a varying drag coefficient depending on the Reynolds number as it is considered constant. To realize how much of an error this produces, if a constant drag coefficient of 1 is used (the value P. Soule uses in his 1972 study), the total drag force is:

$$D = C_D \frac{n \cdot Diametre \cdot R}{3} \cdot \frac{\rho}{2} \cdot v^2 = 18{,}99N \quad (Cd = 1)$$

As can be seen this produces an error of 25% when compared to the previous accurate calculation taking into account a variable value of the drag coefficient.

4.3.1.1. Supported Line Drag

However, the next calculation of P. Soule's study can result very useful. In order to calculate which percentage of the line drag the model has to carry (some is carried by the handle), the moment of the drag forces can be calculated about the centre of rotation and then divided by the flight circle radius, as seen in Eq 4.15.

$$D = \frac{1}{R} n\int_{x=0}^{x=R} x \cdot C_D \cdot Diametre \cdot \frac{\rho}{2}\left(\frac{v \cdot x}{R}\right)^2 dx = C_D \frac{n \cdot Diametre \cdot R}{4}\frac{\rho}{2} \cdot v^2 \qquad (Eq\ 4.15)$$

This results model having to carry 75% of the previously calculated drag force, since now the effective frontal area of the lines is a fourth of its total projected area. This approximation will be used for the accurate case, in other words, out of the total drag force calculated taking into account a variable drag coefficient, it will be assumed that 75% of it is carried by the model, which will be called supported line drag, and the remaining 25% is to be carried by the handle.

4.3.1.2. Yaw

Having calculated which percentage of the drag force the model has to carry (75% of 15,14N), the resulting forces that are acting on the wing tip of the model can be properly plotted, these are the supported line drag and the line tension.

If it wasn't for the drag force, line tension would be perpendicular to the trajectory of the model,

having only to counterbalance the effect of the centripetal force. Due to this, if we compute the resulting force of the sum of supported line drag and line tension, a resulting force can be found, which will be the real line tension the lines are submitted to.

Supported line drag will be calculated as 75% of the line drag calculated in section 4.1 and line tension was calculated in Chapter 3 when using NASA's catenary arches equations (Eq 3.4). The resulting real tension can be easily calculated using, again, the Pythagoras theorem (Eq 4.16).

$$Real\ Tension = \sqrt{Line\ Tension^2 + Support\ Line\ Drag^2} \qquad (Eq.\ 4.16)$$

$$Real\ Tension = \sqrt{167{,}84^2 + (0{,}75 \cdot 15{,}14)^2} = 168{,}44\ N$$

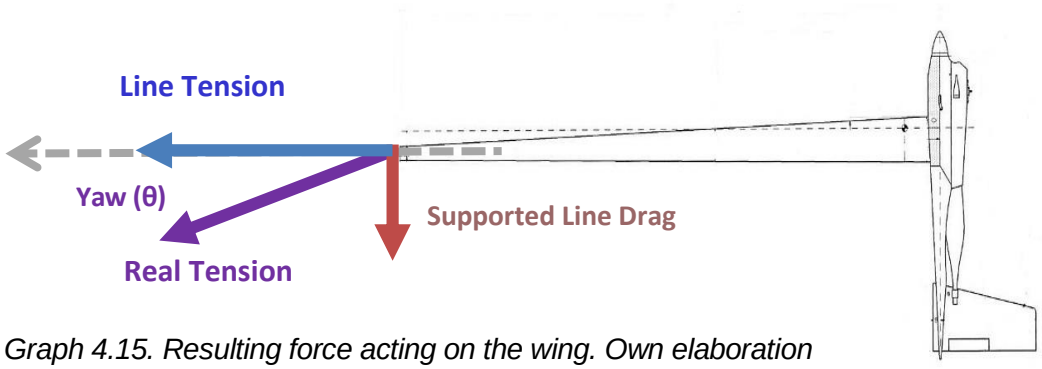

Graph 4.15. Resulting force acting on the wing. Own elaboration

Further than just a value of the real line tension, this calculation can also give is the resulting angle at which this tension is applied, which will be the actual yaw angle at which the model is flying, since the lines are perpendicular to the model's axis of thrust until its centre of gravity. This simple calculation (Eq 4.17) is only possible if the other forces acting on the model are neglected, which would be wing, fuselage and stabilizer drag. Due to their small values in comparison to the tension of 168,4N, this hypothesis has been considered valid.

$$Yaw = \tan^{-1}\left(\frac{Supported\ Line\ Drag}{Line\ Tension}\right) = 0{,}07\ rad = 2{,}58° \qquad (Eq\ 4.17)$$

4.3.1.3. The Lines' Shape

To find out how the lines bend when they are stretched during flight, it is obvious that the two forces which take relevance are the distributed drag along the lines, and the tension at its ends.

In order to simplify calculations, they will be studied separately, and it will be shown that one is significantly more relevant than the other.

Firstly, for the effect that the distributed drag has on the lines, the starting point is Eq 4.4 which gives the differential drag force along the length of the lines. If this force is divided by mass, it can give an expression of each section's acceleration, following Newton's second law of motion. (Eq 4.18)

$$\sum \vec{F} = m \cdot \vec{a} \qquad (Eq\ 4.18)$$

For this study, and only including drag:

$$\frac{0{,}0096x^2 + 0{,}0063x - 0{,}0439}{m} = a(x) \qquad (Eq\ 4.19)$$

Hence, this is an expression of the acceleration of each differential section of the lines. To find out the position and curvature of these, Eq 4.19 must be integrated twice in order to find each section's position (y(x)).

$$y(x) = \iint \frac{0{,}0096x^2 + 0{,}0063x - 0{,}0439}{m} dx =$$
$$= \frac{1}{m}\left(\frac{0{,}0096x^4}{12} + \frac{0{,}0063x^3}{6} - \frac{0{,}0439x^2}{2} + K1 \cdot x + K2\right)$$

Where m is differential mass, therefore it's the section of the wire times the material's density. Since stretching due to tension is being neglected, it will be considered that both ends of the lines are in the y = 0 position, so the arching starts and finishes at either end. Applying these boundary conditions, Eq 4.20 can be obtained, where R is total length of the lines.

$$y(0) = 0\ and\ y(R) = 0, \qquad (K2 = 0)$$

$$y(x) = \frac{1}{m}\left(\frac{0{,}0096x^4}{12} + \frac{0{,}0063x^3}{6} - \frac{0{,}0439x^2}{2} - \left(\frac{0{,}0096R^3}{12} + \frac{0{,}0063R^2}{6} - \frac{0{,}0439Rx}{2}\right) \cdot x\right) \quad (Eq\ 4.20)$$

However, as stated previously, this equation does not take into account the effect of line tension. Nevertheless, if plotted, it can be a good first approximation of what the appearance of the curvature of the lines might be, regardless of the scale. Similar to how tension determines the elongation of a catenary arch, in this case, tension will indicate the scale of the curve obtained. For this reason, a correction factor (K) has been added at the end of the equation to compensate for tension, so the equation found on the *Curve* tab of the excel worksheet is Eq 4.21:

$$y(x) = \frac{1}{m}\left(\frac{0{,}0096x^4}{12} + \frac{0{,}0063x^3}{6} - \frac{0{,}0439x^2}{2} - \left(\frac{0{,}0096R^3}{12} + \frac{0{,}0063R^2}{6} - \frac{0{,}0439Rx}{2}\right)\cdot x\right)\cdot\frac{1}{K} \quad (Eq\ 4.21)$$

To have a better understanding of what influence the value of K has on the shape of the lines, graph 4.16 shows possible outcomes.

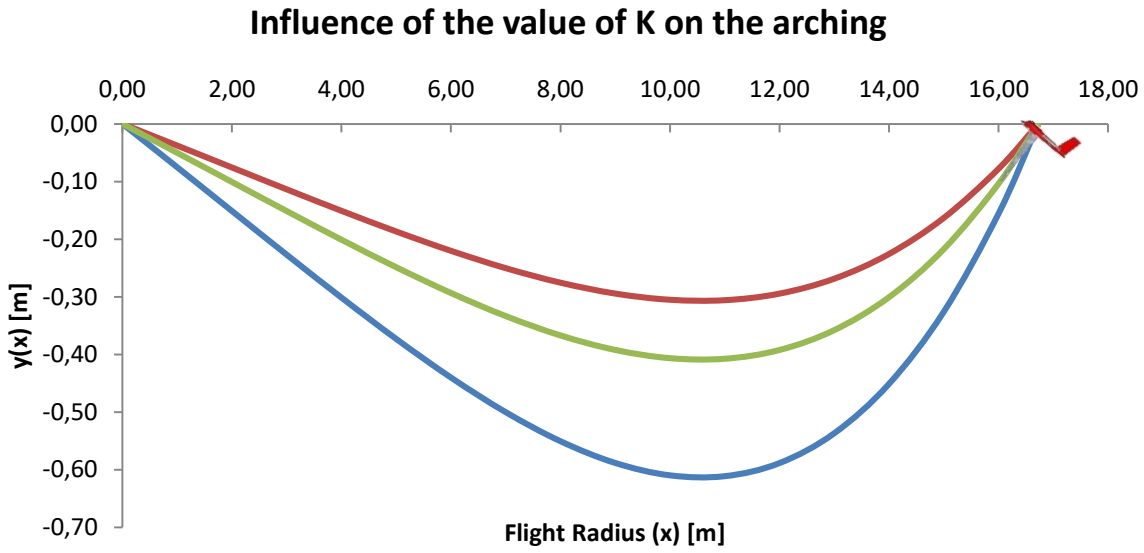

Graph 4.16. Different arching values due to the variation of K. Own Elaboration

It is clear that by changing the value of K, the curve is emphasized or diminished, so in order to find out which of these curves is the correct solution for this study, calculations involving yaw regain importance. Previously in chapter 4, yaw (θ) was calculated to be of 2,58°. In graph 4.16, that value would correspond the angle between the wing of the model and the horizontal axis. Again, using iteration methods made easy by the excel worksheet, the value of K can be modified until the desired yaw angle is obtained. This angle is calculated using the last two plotted values of the curve, and since they are about 700mm apart, they are a decent enough indication of the angle that the lines approach the model at.

For the tension previously calculated, K's value is 237000 to obtain the desired yaw of 2,58° as can be seen in graph 4.17, which shows the resulting curve obtained.

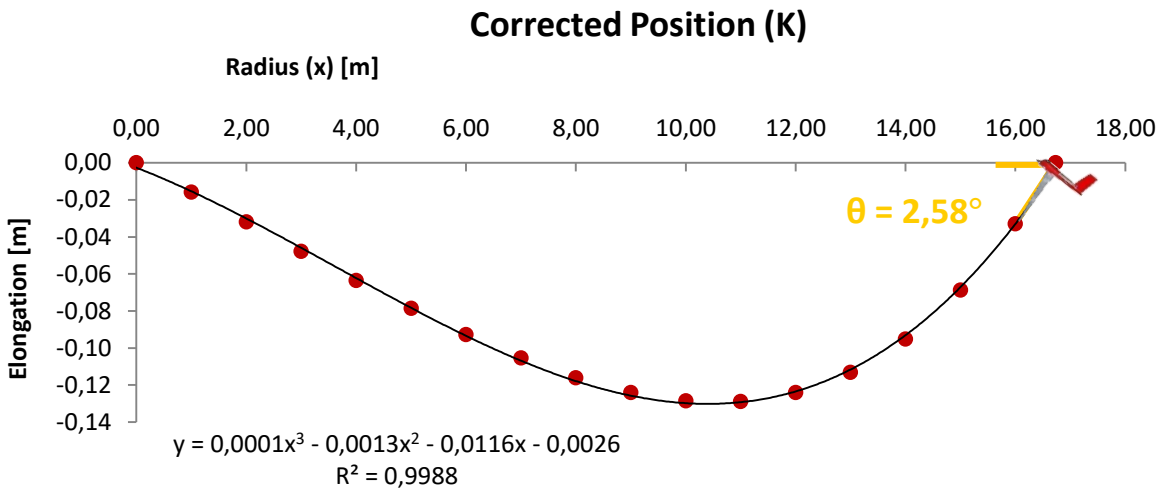

Figure 4.17. Expected arching to produce a yaw angle of 2,58°. (not to scale). Own Elaboration.

As can be observed, despite both axes not being in the same scale, this representation allows the comparison of how drag has a stronger influence away from the centre of flight, since the maximum distance the line strays from its rectilinear projection is at 11m. This deviation has a value of around 140mm, which, when compared to the total line length of 16730mm is quite insignificant. To prove the insignificance of this curvature, the length of the arc can be calculated using Eq 4.22. which will use the equation which best fits the described curve, in this case a third degree polynomial (Eq 4.13)

$$Length\ (L) = \int_{x=0}^{x=16730} \sqrt{1 + \left(\frac{dy}{dx}\right)^2} \quad [mm] \qquad (Eq\ 4.22)$$

$$y(x) = 0{,}0001x^3 - 0{,}0013x^2 - 0{,}0116x - 0{,}0026 \qquad (Eq\ 4.23)$$

$$L = \int_{x=0}^{x=16730} \sqrt{1 + (0{,}0003x^2 - 0{,}0026 - 0{,}0116)^2} = 16731{,}72mm$$

So the shortening in line length due to arching is:

$$16731{,}72mm - 16730mm = 1{,}72mm$$

Now, the stretching due to the line's elasticity must be calculated so in order to compare how much the radius is shortened by the curvature of the lines to how much the stretching of these causes the radius to increase. To be able to proceed, it is important to know the value of Young's modulus (E).

4.3.1.3.1 Young's Modulus

The Young's modulus (or elastic modulus) is the rate at which a linearly elastic material stretches and relates stress and strain. To be precise, this modulus is the slope of the linear segment obtained from the stress-strain curve.

For this study, the value of E for the lines is needed, and since these can be made up of two similar materials, piano wire or stainless steel, two samples of each of these lines were tested in the University's laboratory in order to obtain a better approximation of E. The desired values would have to be somewhere around 200 GPa for the stainless steel wire (AISI 304) and 210GPa for the piano wire, as stated in their material characteristics specifications found online (Acerinox, 2013).

The test was done by holding each wire by its two ends using cylindrical clamps at either ends, as can be seen in Figure 4.18. Then, an Instron 3367 testing system, would apply traction from both ends gradually as it records the force used and the stretching caused by it. These were the two outputs of the machine, which were recorded on an Excel sheet until the wire snapped. If the force is then divided by the section of the wire, and the stretch is divided by the initial value of the length of the wire, stress and strain can be calculated, respectively.

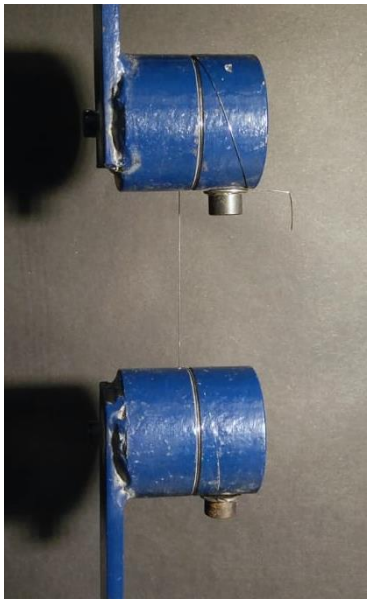

Figure 4.18. Piano Wire Traction Test

If stress-strain curves are plotted for each type of wire (Annex 1.3 and 1.4), the slope of the linearly dependent segment was nowhere near the expected values. These were of 46GPa for the piano wire and 31GPa for the stainless steel wire, around a 15%-20% of the expected value.

A number of possible sources of error were thought up and the most relevant seemed to be that the initial length of the wires was not just the straight part of the wires but also included some of the bent wire around the clamps. Various university staff including Dr. Francesc Roure and Francesc Joaquim Garcia were consulted and despite their agreement in the small importance of the stretching around the clamps, it was discussed that a new test with a greater

initial separation of the clamps would diminish any possible influence.

Thus, a new test was carried out by separating the initial distance of the clamps for both wires; resulting in an initial length of 250mm instead of the 120mm of the first test. Additionally, the end of the straight segment of the wire was marked with a white marker in order to observe how much stretching was occurring at the tip. After the second test, this was visually determined to be around a millimetre and despite its small value, it was added to the total initial length value and new stress-strain curves where elaborated which can be consulted in Annex 1.5 through Annex 1.8. The resulting Young's modulus were of 59GPa for the stainless steel and 74GPa for the piano wire.

This great divergence between the elastic modulus cited in material properties literature and the resulting experimental values, called for a deeper research of the variation of elastic properties for thin wires, and even though this should have been done before testing the wires, thankfully, studies where found contemplating the same phenomenon. Fallen et al (2002), concludes in his study *Measuring the elastic properties of fine wire* that due to the cold working required to manufacture such thin wires, the Young's modulus of these could end up resulting of as little as 26% of the expected value. The latest values found in the second test were of 30% for the stainless steel and 35% for the piano wire, so it fit with that hypothesis. For this reason, the values of 59GPa for stainless steel wire and 74GPa for piano wire, have been considered as valid

4.3.1.3.2 Line Stretch

Therefore, different stretch values will result from each line material, so these can be studied side by side. Eq 4.24 which derives from Hooke's Law relates the elongation of the lines with the force applied to them (tension), their section, and their elasticity modulus. Notice how in Eq 4.25 and Eq 4.26, line tension is divided by two, since there are two control lines taking the model around the circuit, so each line has to carry half of the tension.

$$\varepsilon = \frac{\sigma}{E} \quad \rightarrow \quad \Delta l = \frac{F}{S}\frac{l_0}{E} \qquad (Eq\ 4.24)$$

For piano wire:

$$\Delta l = \frac{F}{S}\frac{l_0}{E} = \frac{167{,}84N/2 \cdot 16{,}73m}{1{,}26 \cdot 10^{-7} \cdot 74 \cdot 10^{9}Pa} = 0{,}15m = 150{,}98mm \qquad (Eq\ 4.25)$$

For stainless steel wire:

$$\Delta l = \frac{F}{S}\frac{l_0}{E} = \frac{167{,}84N/2 \cdot 16{,}73m}{1{,}26 \cdot 10^{-7} \cdot 59 \cdot 10^{9}Pa} = 0{,}19m = 189{,}37mm \qquad (Eq\ 4.26)$$

If this stretching is compared to the shortening of the wires due to drag force, it is clear that the shortening barely accounts for 1% of the stretching involved due to tension. For this reason, and to simplify calculations, only the stretching of the cables due to their elasticity will be taken into account to compute the new true flight radius.

It is also worth mentioning that stretching could cause the wires to reduce their diameter due to the conservation of mass; however, it has been calculated that the new diameter would be around 0,398mm thick, an insignificant change to the initial 0,4mm.

4.4. True Flight Radius

Therefore, if piano wires were used, the line stretch would be of 150,98mm, so if the model is considered to be a rigid solid, the total distance from the centre of the flight radius to the centre of gravity of the model would increase in this precise amount, so the new flight radius would be 17,627m + 0,151m = 17,778m. Similarly, for the stainless steel wire, a more elastic material, the true flight radius would be 17,627m + 0,189m = 17,816.

These variations will have considerable effects on the performance of the model, which will be addressed under *Overall Performance.*

Once the yawing tendency of the model has been studied, and the results on the true fight radius summed up, it is just as important to analyse the pitching moment. Pitching, or as otherwise commonly known, nose-up or nose-down tendency, in control line, is caused by the interaction of three moments: The moment of the own weight of the model, the moment created by the lift force, and the element which creates a great divergence between control line and other types of aviation modelling and aviation in general, the moment created by the gyroscopic effect.

5. Model Pitch

5.1. Understanding the forces involved in creating pitch

Usually, one studies moments about the centre of gravity of on object, so that its own weight does not create a moment from that point. For this study however, perhaps the most complex force is lift. Due to this, moments will be studied around the aerodynamic centre of the aerofoil, here is why.

5.1.1. Lift

Lift is the aerodynamic force which unlike drag, acts perpendicular to the flow of a fluid, in this study, air. It can act both against gravity, like in the case of aerofoils on aircraft wings, or in the opposite direction. The latter case is more commonly known as downforce, for example used in front and rear wings of racing cars, to gain traction to the track.

In this thesis, lift is contemplated as an upwards force generated by the geometry and the angle of attack of both the stabilizer and the wing aerofoils, as mentioned in Chapter 3 when calculating the angle of attack. It will be assumed that the total lift force is generated in the aerodynamic centre of the wing, which will account for most of the lift force generated.

For a symmetrical aerofoil flying at subsonic speeds, the aerodynamic centre is located approximately at 25% of the chord length, and its location doesn't vary with the angle of attack (N. Hall, 2015). Furthermore, at that point, it has been theoretically and empirically proven that aerodynamic momentum doesn't significantly change with the angle of attack. So for the NACA0012 aerofoil, which is a symmetrical model, aerodynamic moment is null for all angles of attack at 25% of the chord. This is why it is important to study the sum of moments around the aerodynamic centre: if lift is considered to be applied at that point, only weight and the moment induced by the gyroscopic effect will contribute the total pitching moment, as can be seen in Figure 5.1. The contribution of these two will now be explained in detail.

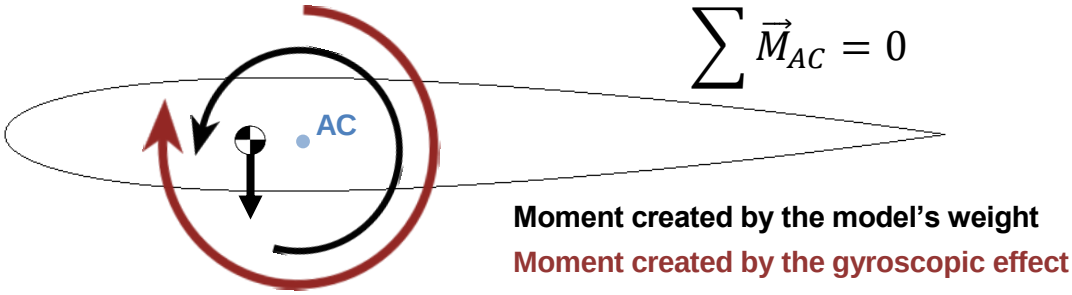

Figure 5.1. Moments involved in creating pitch around the aerodynamic centre.

5.1.2. Weight

The moment created by the weight of the model is easy to compute. It can be found simply by multiplying the weight times the distance from its point of application (Centre of Gravity) to the aerodynamic centre.

5.1.3. Gyroscopic effect

Perhaps one of the less understood results of flying a model on a circular flight, is the gyroscopic effect, resulting from the rotating propeller (and other associated rotating components), when in turn, they move on a circular path.

The variation in direction of the axis of rotation of the propeller and its associated parts creates a reaction which takes places at 90 degrees after the direction of rotation, hence the pitching, or nose-up tendency. This is due to the conservation of angular momentum, a phenomenon widely used in, for example, navigational systems, smartphone gyroscopes and even the Hubble telescope.

This phenomenon is usually studied in the opposite scenario. If a real life-size single-propeller aircraft pitches up or down with its elevator tail tabs, the resulting action, called precession, makes the aircraft yaw to the left (assuming a clockwise spinning propeller), as can be seen in Figure 5.2. Once the concept of precession is understood, it can be used not only to yaw the aircraft left or right, but also to aid spinning, and other complex manoeuvres usually used in aerobatic flying.

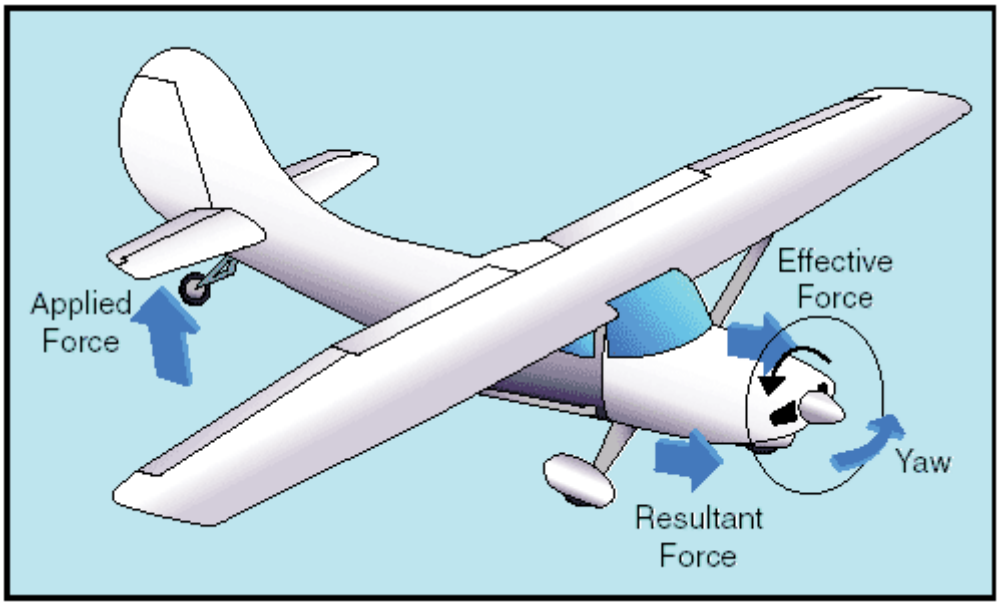

Figure 5.2. Yaw tendency as a result of pitch. Rapp.org

So in order to study the magnitude of this effect, it is important to first know exactly how many components are involved in rotating with the propeller, as well as their moment of inertia.

5.1.3.1. Rotating Parts and their Moment of Inertia

Each F2A can be slightly different, but most work with a single piston combustion engine, which acts on the propeller driven by the crankshaft. The nosecone, which holds the propeller in place, also rotates at the same speed, and itself consists in three parts fitted together. All of the mentioned rotating parts, for the *Barcelona 96* model, have been modelled using Dassault System's SolidWorks software in order to calculate their rotational inertia.

By creating an assembly of these parts (Fig. 5.2), and then an exploded view, their interaction with one another is clearer, as can be seen in Figure 5.3.

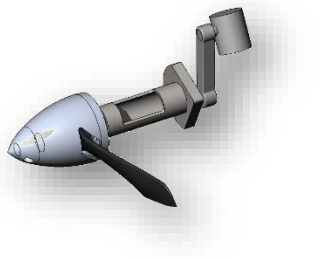

Fig. 5.2 Assembly

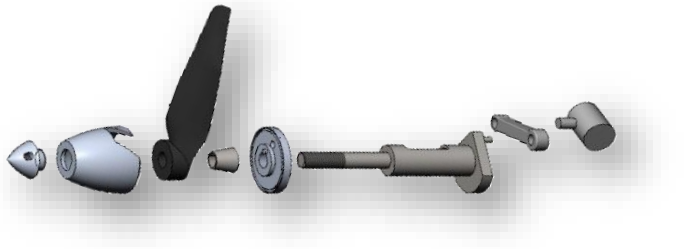

Fig. 5.3 Exploded View of the Assembly

As can be seen, there are two parts that have been modelled but do not revolve around the propeller's axis of rotation; they are the piston of the of combustion engine, and its connecting rod. These correspond to the right-most parts of Figure 5.3. They have been modelled purely to better comprehend the whole systems' functionality, but they only contribute to generating small vibrations along the model, and do not produce a gyroscopic effect (J. Supercool, 2013).

By adding the according material properties to the parts via SolidWorks, and if the parts are constructed using the axis of rotation as one of the primary axis of the SolidWorks' Coordinate system, the moment of inertia along the desired axis can automatically be computed by the program. This data for each rotating part has been introduced in the *Inertia* tab of the Excel worksheet.

The only relevant property for calculating moments of inertia is density, as the first is given in $grams \cdot mm^2$. For the two cones and the disk, the material was aluminium (density of 2,7g/cm^3); for the crankshaft and small joint the material was steel (density of 7,9 g/cm^3) and the propeller was made out of ABS plastic (density of 1,1 g/cm^3).

5.1.3.2. Resulting Moment

Once the moment of inertia has been found for each rotating part, the moment created by these can be easily calculated using the formula of the moment for a gyroscope. This would result in multiplying their combined moment of inertia (I) times the angular velocity of the rotating parts, 38000 min^{-1} (Ω1), and by the angular velocity of the model around the circuit (Ω2). (J. Supercool, 2013).

This simplified case is only possible if it is considered that the model is flying perpendicularly

to the wires, and therefore so is the propeller's axis of rotation. This assumption will be made in order to avoid projecting angular velocities. The only unknown variable is now the direction of the resulting moment. As stated it will be 90° after the direction of rotation but its precise direction can be found my multiplying the angular velocities in an established coordinate system:

x axis: Direction of the thrust axis of the propeller.
y axis: Vertical axis (up direction).
z axis: Direction of the lines from the pilot to the model.

Therefore, $\overrightarrow{\Omega 1} = (\Omega 1, 0, 0)$; $\overrightarrow{\Omega 2} = (0, \Omega 2, 0)$

And the resulting direction of the precession moment created:

$$\overrightarrow{\Omega 1} \times \overrightarrow{\Omega 2} = \begin{vmatrix} \vec{x} & \vec{y} & \vec{z} \\ \Omega 1 & 0 & 0 \\ 0 & \Omega 2 & 0 \end{vmatrix} = (\Omega 1 \cdot \Omega 2)\, \vec{z}$$

Therefore, the resulting moment will act in the positive direction of axis that follows the lines, in other words, it will create nose-up pitching moment. Table 5.4 collects the resulting moments for each part using Eq 5.1, and then adds them to obtain the total moment created by the whole assembly (Resulting M). This table can also be found under the *Inertia* tab of the Excel worksheet.

$$\vec{M} = I \cdot \left(\overrightarrow{\Omega 1} \times \overrightarrow{\Omega 2}\right) \qquad (Eq.\,5.1)$$

Ω1	**3979**	rad/s
Ω2	**4,767**	rad/s

Parts		Inertia (I)		Moment (M)		Resulting M	
	**Propeller**	**2491,3**	g · mm²	**4,73E-02**	Nm	**7,10E-02**	Nm
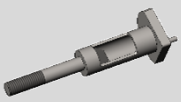	**Crankshaft**	**917,6**	g · mm²	**1,74E-02**	Nm		
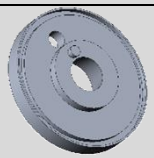	**Disk**	**665,9**	g · mm²	**1,26E-02**	Nm		

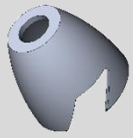	**Large Cone**	**290,1**	g · mm²	**5,50E-03**	Nm
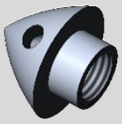	**Small Cone**	**25,2**	g · mm²	**4,77E-04**	Nm
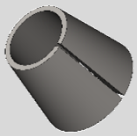	**Joint**	**16,5**	g · mm²	**3,13E-04**	Nm

Table 5.4. Inertia Moments for all rotating parts, and their resulting moment. Own Elaboration.

Therefore, the resulting moment of all of the rotating parts is 0,071 Nm. As stated previously, in order for the model to be at balance, this moment has to compensate for the moment created by the model's own weight around the aerodynamic centre, hence the ideal position of the model's centre of gravity can be found using a simple addition of moments (Eq 5.3). This is true as long as the fuselage's aerodynamic centre falls in the same plane as the wing, so it does not create a pitching moment itself. Due to the symmetry of the model (see Fig 5.2), and both wing and stabilizer intersecting this symmetry plane, this has been considered a valid hypothesis. The possible outcomes if this was not true will be addressed in Chapter 7, under *Improvements.*

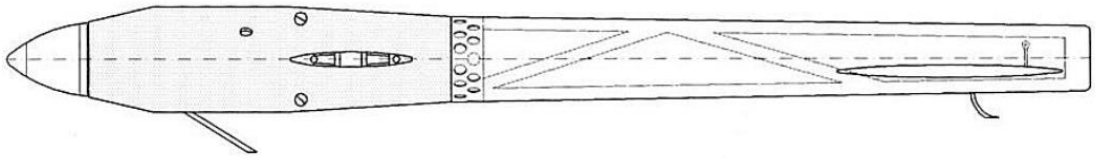

Figure 5.2 Fuselage Section with its symmetry plane plotted.

$$\sum \vec{M}_{AC} = 0 = \vec{M}_{Weight} + \vec{M}_{Gyroscopic} = \quad (Eq\ 5.3)$$

$$= 0{,}42Kg \cdot\ 9{,}81\frac{m}{s^2} \cdot Distance\ from\ AC = 0{,}071Nm$$

$$\hookrightarrow Distance\ from\ AC =\ 17{,}22\ mm$$

Surprisingly, the centre of gravity needs be 17,22 mm in front of the aerodynamic centre of the aerofoil, but since the aerofoil is only 15mm behind the leading edge (25% of the chord) it means the centre of gravity of the model should in fact be in front of the leading edge of the wing (Figure 5.5). This is not the case for the *Barcelona 96* model, as the centre of gravity is very close to the aerodynamic centre, at 15,5mm from the leading edge. So this inconsistency will be addressed under improvements and conclusions.

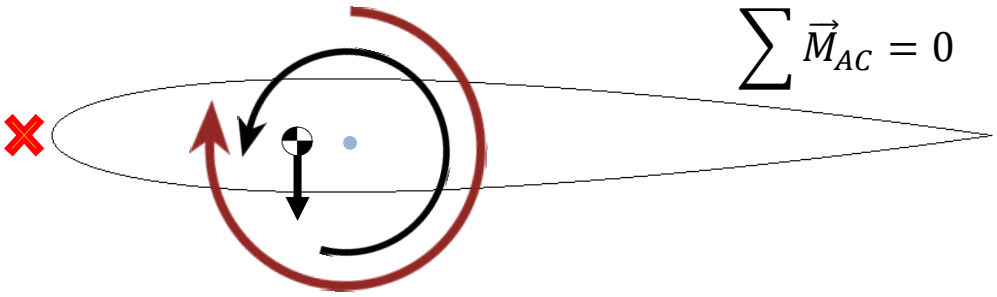

Figure 5.5. Ideal placement of the model's centre of gravity (red cross).

6. Overall Performance

Finally, in the *Output* tab of the worksheet, there is a compilation of relevant data calculated throughout the study. The first table (6.1) compiles the most relevant forces involved in the mechanical study of the model, as well as the pitching moment which should be compensated with the placement of the centre of gravity.

Tables 6.2 and 6.3 give the total power output required from the engine and the flight angles of the model, respectively.

Forces and Moments		
Lift	29,66	N
Line Drag	15,14	N
Supported Line Drag	11,36	N
Model Drag	3,46	N
Total Drag	23,24	N
Tension	167,84	N
Centripetal Force	168,93	N
Pitching Moment	7,10E-02	Nm

Table 6.1. Forces and Moments Output

Engine		
Power Required	1358,38	W

Table 6.2. Engine Performance

Flight Angles		
Yaw	2,58	degrees
Pitch	1,29	degrees
Roll	5,49	degrees

Table 6.3. Flight Angles Output

Furthermore, Table 6.4, perhaps the most important one of the worksheet, calculates the official speed that would be recorded considering the parameters introduced. For example, due to stretching, despite the linear speed of the model is known because it depends on the engine capacity, the increase in flight radius would lengthen the time taken to complete 9 laps and thus the official timed speed by the FAI would be lower. Table 6.4 shows exactly how much that speed is decreased due to the use of different types of lines.

	For Piano Wire		For Stainless Steel Wire	
Stretch	150,98	mm	189,37	mm
Flight Radius	17,78	m	17,82	mm
Model Linear Speed	302,50	km/h	302,50	km/h
Angular Velocity	4,73	rad/s	4,72	rad/s
Recorded Speed	**301,00**	**km/h**	**300,35**	**km/h**

Table 6.4. Recorded Speed due to the use of different types of lines.

7. Improvements

7.1. Flight Radius

As can be observed in Table 6.4, due to the variation in the flight radius, the model is in fact flying at a greater distance from the pilot than the established 17,69m. If it is considered that the linear speed of the model is determined by the engine's capacity, therefore it is constant, due to the increased radius of flight, the angular velocity decreases. This goes against the interests of the pilot, since results in official timed effort would calculate speed using a radius of flight of 17,69m. Therefore, recorded speed flying with the more elastic lines, stainless steel wires, produce worse results than flying with more rigid lines made out of piano wire. The difference observed in table 6.4 might seem small (300km/h versus 301km/h) but in a competition where world records are counted by the tenth of a second, it makes quite the difference.

Thus, it is optimal to use lines with the greatest possible elastic modulus, even if their weight is increased, as it has been demonstrated that sagging due to the lines' own weight is not even close to having and influence.

7.2. Centre of Gravity

Having calculated the necessary location of the model's centre of gravity to compensate for the pitching moment created by the gyroscopic effect it is important to understand why this has been done.

The model *Barcelona 96* has an initial non-existent angle of attack, in other words, both the wing and the stabilizer are parallel to the plane of flight and their chords are parallel to each other. This means that in order to produce the minimum drag, the plane should be close to being level to the ground, only generating enough lift to be kept in flight. This is why the pitching moment needs to be completely compensated.

However, a configuration with a wing and stabilizer that are not parallel to each other could introduce much more flexibility when choosing an angle of attack. For example, if the lift generated from both stabilizer and wing could be exclusively generated by the wing, the stabilizer could remain parallel to the plane of flight, and therefore reduce its drag. This drag generated by the rear stabilizer is what is known as trim drag. On the other hand, trim drag could be used to the advantage of the pilot, with a negative angle of attack.

If the stabilizer is placed slightly downwards, (negative angle of attack), the downforce generated at the rear could be used to compensate the nose-up tendency of the propeller, thus enabling more flexibility in the placement of the centre of gravity of the model, which cannot always be placed wherever. However, this increases trim drag, so it would be optimal to find a balance between creating a nose-heavy model and generating a slight downforce with the stabilizer. Furthermore, too much downforce generated by trim drag on the stabilizer would create much sharper turns when controlling the model, as the flaps used to control the model's height are also located in the rear stabilizer.

In fact, these flaps could be controlled mid-flight to compensate for the pitching moment, so as well as controlling the height of the model, it also controls its pitching angle, more flexibly than creating a model with a fixed pitch on the stabilizer. This is a possible reason for the *Barcelona 96* model to have its centre of gravity so far back, because it can compensate the pitching moment constantly with its flaps.

Studying these possible variations with different models could result costly and very time-consuming, for this reason, it is important to see exactly how much this project can cost if carried out from scratch.

8. Budget

The total budget of the project has been calculated according to table 8.1:

Concept	Units	Cost
Control Line Wires for Testing	1m (x2)	2 €
Microsoft Office Home & Student 2016 License	1	149 €
SolidWorks Standard License	1	3395 €
Personal Computer capable of running CAD Software	1	~ 500 €
Instron 3367 Universal Testing System	1	~ 15 000 €
Workload	360h	7200 €
Total Cost		**~26 250 €**

Table 8.1. Cost of the project broken down by items.

Despite most of the cost originating in software licenses and expensive heavy-duty machinery, these are all used to find mechanical properties of model parts and lines. If these properties can be directly inquired to the manufacturer (when possible), the cost of this project would be reduced considerably, and furthermore, once the properties have been found once, it is unlikely that some parts need to be tested again. For example, it is uncommon to use lines that are not either piano wire or stainless steel wire, so once their generic elastic modulus for 0,4mm wires has been found and possibly shared among enthusiasts, the 15 000€ expense of the testing system could be spared.

9. Environmental Impact

Like in most combustion engines, the products of the chemical reaction that takes place inside the cylinder are not always desirable. For the case of F2A control line racing, the composition of the fuel used is strictly regulated in the sporting code, stating that it must be composed of 80% methanol and 20% castor oil. The resulting biodiesel produces carbon dioxide when combusted, one of the major greenhouse gases. Despite the small scale of a control line model, without the use of the Excel sheet provided with this study, there would be a greater number of test runs needed in order to know the performance of each model. For this reason, the study contributes to reducing greenhouse emissions by reducing time spent testing the models.

Figure 9.1. An example of a prepared mix of fuel specifically created for control line. MorganFuel

On top of the gas pollution created by the engine, the high rotational speed at which these perform, produce a very distinctive and loud noise. Acoustic pollution therefore is also a result of control line flying and for this reason most circuits are located in the outskirts of towns and cities, and not near housing. For the case of Barcelona, the circuits are located in the hill of Montjuïc, surrounded by trees which offer some protection and project the soundwaves mostly upward. Nevertheless, when speed models are being flown, the sound of the engines can be heard even from several hundred meters away.

Conclusions

Throughout this study, the following conclusions have been drawn, in order of appearance during the report:

The catenary arching of F2A lines due to their own weight is close to null, therefore these can be approximated to being straight in the vertical axis.

Most of the drag force which the pilot has to counter with its model is generated by the lines, which despite their reduced diameter, their considerable length makes them account for 65% of the total drag. This drag acts on the lines following a second degree polynomial equation which results in a noticeable line arching along the plane of flight. However, the reduction in flight radius caused by this arching is small compared to the lengthening of the radius due to the lines stretching elastically. This stretching depends on the lines' elastic properties and it has been proven that using stainless steel wire will increase the flight radius more than with piano wire.

Since drag force on the wires is the greatest hurdle in the goal to achieving high speed, and this force is directly related to air density, clear summer skies would be optimal for establishing new world records, as the high temperatures combined with low atmospheric pressures will contribute to diminishing air density and thus, drag.

The total power need to keep the model in flight at the speed of 302,5km/h is greater than the manufacturer's theoretical output power, so it is possible this value is incorrectly given by the manufacturer, or the engine had been tampered with in order to increase its performance.

If the model is set to fly with its wing and the rear stabilizer parallel to each other, a nose-heavy model is needed, in order to compensate for the pitching moment created by the rotating parts of the model. However, this can be avoided by tilting the wing and stabilizer at different angles of attack thus creating various pitching moments that counteract.

The excel program has proven to be efficient as, many times, certain incorrect values had to be changed once the project had started and the interaction between the cells allowed for automatic updates. As mentioned, the output parameters can be iteratively introduced in the program again as flight radius varies, and so does drag, lift, and so on. The close links between different aerodynamic and mechanical theorems involved, make it surprisingly difficult to study any single phenomenon by itself. Hence the importance of being able to quickly re-do a whole

study if some parameters are changed.

Due to the costly budget of this project, carrying out this study would only be suitable for enthusiasts who are willing to test multiple variations of their models and improvements, as the are many fixed initial costs which only become less relevant as many studies are carried out.

Further Actions

It would be of great interest to measure with improved accuracy the elastic modulus of the lines, as their stretch is one of the most important parameters regarding the models' performance. In this study, only a couple of tests could be done with each line, and using old clamps on a machine that was clearly not designed for testing such thin wires (the maximum machine load was 30kN of which roughly only 300N were used).

Acknowledgements

First of all, I would like to thank my tutor Lluís Roger for introducing me to the world of control line, and mentoring me throughout my thesis. His enthusiasm in the subject was clear and he provided me with various resources dating many years back which otherwise would have been almost impossible to find on my own.

Second of all, I also want to thank Lluís Parramón, for personally showing me around the control line circuit in Montjuïc, and not only emphasizing which parts of the study could be more relevant than others, but also for providing me with parts of his models so that I could test them in the laboratory.

In the mentioned laboratory, I was gladly helped by both Dr. Francesc Roure and Francesc Joaquim Garcia, both of whom I would like to thank for contributing to making me understand and test the properties of the thin control line wires, no easy task.

Lastly, I would like to thank my parents for their continued support throughout not only this thesis, but the whole Bachelor's degree, understanding the challenge it meant, and motivating me through the tougher times. For this reason, my last thanks go to Carol and Ricard for helping me to understand what priorities lie outside of school, and putting everything into perspective.

Bibliography

References (in order of appearance)

D. Macy, F. (1990). *History of the Jim Walker Fireball U-Control Balsa Model Plane - Early Control Line Model airplane from American Junior*. [online] Americanjuniorclassics.com. Available at: http://www.americanjuniorclassics.com/Fireball/fireballhistory.htm [Accessed 5 Mar. 2018].

Olsson, G. (2013). *Introducing Control Line Model Flying*. [online] Go-cl.se. Available at: http://www.go-cl.se/clinf.html [Accessed 5 Mar. 2018].

Fai.org. (2018). *F2 Control Line Sporting Code*. [online] Available at: https://www.fai.org/sites/default/files/documents/sc4_vol_f2_controlline_18.pdf [Accessed 10 Mar. 2018].

Parramon, L. (1997). *The Scoop of the decade for all the F2A types – Complete details on engine, pipe, prop and airplane of the 193MPH FAI world champ.* Speed Times. January-March 1997. Vol 16, Number 1. p. 9-13.

European Environment Agency. (2018). *European Environment Agency's home page*. [online] Available at: https://www.eea.europa.eu/ [Accessed 20 Mar. 2018].

Crane Company. (1988). *Flow of fluids through valves, fittings, and pipe*. Technical Paper No. 410 (TP 410).

Hall, N. (2015). *Kite Sag.* [online] Grc.nasa.gov. Available at: https://www.grc.nasa.gov/www/k-12/airplane/kitesag.html [Accessed 15 Apr. 2018].

Soule P. (1971). *Flight Mechanics of Control Line Wires.* Aeromodeller manual (1971-1972). p. 100-107.

González S. (1976). *Ensayos de modelos de velocidad en túnel de viento.* Escola Tècnica Superior d'Enginyeria Industrial de Barcelona.

Benson, T. (2015). *Centre of Pressure.* [online] Grc.nasa.gov. Available at: https://www.grc.nasa.gov/www/k-12/VirtualAero/BottleRocket/airplane/cp.html [Accessed 14 May. 2018].

Acerinox (2013). *Austenitic Stainless Steel Properites. ACERINOX S.A. Madrid [online] Available at:* http://www.acerinox.com/opencms901/export/sites/acerinox/.content/galerias/galeria-descargas/galeria-documentos-producto/ACX120-low.pdf [Accessed 20 May. 2018].

Fallen J. et al. (2002) *Measuring the elastic properties of fine wire.* John Wiler and Sons Inc. [online] Available at: https://onlinelibrary.wiley.com/doi/abs/10.1002/jbm.1071 [Accessed 20 May. 2018].

Hall, N. (2015). *Aerodynamic Center*. [online] Grc.nasa.gov. Available at: https://www.grc.nasa.gov/www/k-12/airplane/ac.html [Accessed 20 May. 2018].

Supercool, J. (2013). *Control Line: Speed model C/G position*. [online] Supercoolprops.com. Available at: http://www.supercoolprops.com/articles/gyroscope.php [Accessed 15 mar. 2018].

Supercool, J. (2013). *Control Line: Gyroscopic behaviour of propellers*. [online] Supercoolprops.com. Available at: http://www.supercoolprops.com/articles/gyrovibes.php [Accessed 15 Mar. 2018].

Complementary Bibliography

En.wikipedia.org. (2018). *Control line*. [online] Available at: https://en.wikipedia.org/wiki/Control_line#History [Accessed 23 Mar. 2018].

Lee, H. (2011). *About Me: Heman Lee*. [online] Aeromaniacs.com. Available at: http://www.aeromaniacs.com/historyofcl.htm [Accessed 23 Mar. 2018].

Fai.org. (2018). *About us | World Air Sports Federation*. [online] Available at: https://www.fai.org/page/ciam-about-us [Accessed 15 Mar. 2018].

Fai.org. (2018). *F2 Control Line Sporting Code*. [online] Available at: https://www.fai.org/sites/default/files/documents/sc4_vol_f2_controlline_18.pdf [Accessed 15 Mar. 2018].

En.wikipedia.org. (2018). *National Institute of Standards and Technology*. [online] Available at: https://en.wikipedia.org/wiki/National_Institute_of_Standards_and_Technology [Accessed 20 Apr. 2018].

Lmnoeng.com. (2013). *Gas Viscosity Calculator*. [online] Available at: https://www.lmnoeng.com/Flow/GasViscosity.php [Accessed 20 Apr. 2018].

En.wikipedia.org. (2018). *Aerodynamic center*. [online] Available at: https://en.wikipedia.org/wiki/Aerodynamic_center [Accessed 12 Jun. 2018].

Morganfuel.com. (2018). Morgan Fuel. [online] Available at: http://www.morganfuel.com/omega_gallon [Accessed 2 Jun. 2018].

Marlongofast.tripod.com. (2018). *Cylinder Drag*. [online] Available at: http://marlongofast.tripod.com/pdf_files/CylDrag.htm [Accessed 12 May. 2018].

Rapp, R. (2018). *Gyroscopic Precession*. [online] The House of Rapp. Available at: https://www.rapp.org/archives/2008/09/gyroscopic-precession/ [Accessed 10 Jun. 2018].

Clspeed.com. (2018). *North American Speed Society*. [online] Available at: http://www.clspeed.com/ [Accessed 13 Apr. 2018].

En.wikipedia.org. (2018). *Environmental impact of biodiesel*. [online] Available at: https://en.wikipedia.org/wiki/Environmental_impact_of_biodiesel [Accessed 2 Jun. 2018].

Henry J. et al. (1951). *Drag of Control Lines and Models.* 1951-1952 Model Aeronautic Yearbook.

Mh-aerotools.de. (2018). *Aerodynamics of Model Aircraft*. [online] Available at: https://www.mh-aerotools.de/airfoils/ [Accessed 13 Mar. 2018].

Soule P. (1971). *Control Line Level Flight Flight Line Drag and Shape Analysis.*